

Truncation Error Estimation in the p-Anisotropic Discontinuous Galerkin Spectral Element Method

Andrés M. Rueda-Ramírez · Gonzalo Rubio · Esteban Ferrer · Eusebio Valero

Received: date / Accepted: date

Abstract In the context of Discontinuous Galerkin Spectral Element Methods (DGSEM), τ -estimation has been successfully used for p-adaptation algorithms. This method estimates the truncation error of representations with different polynomial orders using the solution on a reference mesh of relatively high order.

In this paper, we present a novel anisotropic truncation error estimator derived from the τ -estimation procedure for DGSEM. We exploit the tensor product basis properties of the numerical solution to design a method where the total truncation error is calculated as a sum of its directional components. We show that the new error estimator is cheaper to evaluate than previous implementations of the τ -estimation procedure and that it obtains more accurate extrapolations of the truncation error for representations of a higher order than the reference mesh. The robustness of the method allows performing the p-adaptation strategy with coarser reference solutions, thus further reducing the computational cost. The proposed estimator is validated using the method of manufactured solutions in a test case for the compressible Navier-Stokes equations.

Keywords High-order discontinuous Galerkin · Spectral methods · p-Anisotropic representations · τ -Estimation · Truncation error · Anisotropic p-adaptation

Mathematics Subject Classification (2000) 65M15 · 65M50 · 65M60 · 65M70

A. M. Rueda-Ramírez · G. Rubio · E. Ferrer · E. Valero
ETSIAE (School of Aeronautics), Universidad Politécnica de Madrid.
Plaza de Cardenal Cisneros 3, 28040 Madrid, Spain.
Tel.: +34 913 3663 26 - Ext. 205
E-mail: am.rueda@upm.es

A. M. Rueda-Ramírez · G. Rubio · E. Ferrer · E. Valero
Center for Computational Simulation, Universidad Politécnica de Madrid.
Campus de Montegancedo, Boadilla del Monte, 28660 Madrid, Spain.

arXiv:1806.08439v1 [cs.NA] 21 Jun 2018

1 Introduction

High-order Discontinuous Galerkin (DG) methods are becoming a popular alternative to low order methods for solving Partial Differential Equations (PDEs) because of their high accuracy and flexibility [47, 6]. Among those, the Discontinuous Galerkin Spectral Element Method (DGSEM) [20, 22] is a nodal (collocation) version of the DG method on hexahedral meshes which allows p-anisotropic representations and has been used in a wide range of applications [22, 34, 26, 7, 12]. In the DG approach, the continuity constraint on element interfaces is relaxed, allowing for discontinuities in the numerical solution. This feature makes them more robust than continuous methods for describing advection-dominated problems, like the ones usually encountered in fluid dynamics. Moreover, DG methods can handle non-conforming meshes with hanging nodes and/or different polynomial orders efficiently, as is necessary for mesh adaptation strategies [36, 22, 11].

Error estimates are a powerful tool in computational sciences as they quantify how accurately a numerical solution satisfies the governing mathematical equations [27, 37, 39]. A precise assessment of the numerical errors is useful for defect correction (a technique that enables high accuracy by correcting the numerical solution using an estimation of the error [37, 23]), or for guiding mesh adaptation strategies [48, 24, 25]. The former requires highly accurate estimates of the discretization error and, therefore, a significant amount of computational resources is usually invested in computing them [31]. The latter has been broadly studied in the literature. In particular, the most common approaches are the *adjoint-based* adaptation [8, 16, 15, 46, 33], where the numerical error of a functional (e.g. lift or drag) is estimated, which involves a high computational cost; the *feature-based* adaptation, which relies on on easy-to-compute adaptation criteria, such as the assessment of jumps across element interfaces in the case of DG discretizations [35], or the identification of large gradients [1, 28]; and the *local-error-based* adaptation [24, 25, 2, 13, 43, 44, 19, 18], which depends on the assessment of any measurable local error in all the cells of the domain. A detailed comparison of the different approaches for error estimation and adaptation can be found in [13] in the context of finite volumes or [19] for high-order DG schemes. The *local-error-based* adaptation methods are interesting since, in contrast to *feature-based* methods, they provide a way to predict and control the overall accuracy, and are computationally cheaper than *adjoint-based* schemes [19, 18]. The topic of our work is the development of an accurate and cheap local error estimator to drive p-anisotropic adaptation in the DGSEM.

Two different errors are particularly relevant. On the one hand, the discretization error is the most important, but also the most difficult error to estimate [31]. It is defined as the difference between the exact and numerical solutions to the problem and can be approximated by means of solving the Discretization Error Transport Equation (DETE) [26], an auxiliary PDE whose approximation involves the investment of further computational resources. Some of the first works using estimations of the local discretization error in high-order methods were proposed by Mavriplis [24, 25], who developed hp-adaptation techniques for the Spectral Element Method, and Casoni et al. [9], who used a similar approach to evaluate where to add artificial viscosity for shock capturing in Discontinuous Galerkin dis-

cretizations.

On the other hand, the truncation error is defined as the difference between the discrete partial differential operator and the exact partial differential operator,

$$\tau(\cdot) = \mathcal{R}^N(\cdot) - \mathcal{R}(\cdot), \quad (1)$$

and is usually evaluated for the exact solution of the PDE [31, 41, 18, 19]. The truncation error is related to the discretization error through the DETE [39], where it acts as a local source term. This relation makes it useful as an indicator for mesh adaptation methods [43, 5] since refining the mesh where the truncation error is high reduces the discretization error in all the mesh [41], with an additional advantage: the truncation error estimation requires less computational effort. Furthermore, in hyperbolic problems the discretization error is strongly advected, i.e. it is transmitted downstream from under-resolution areas, but the truncation error is only weakly advected. Therefore, an adaptation procedure based on the truncation error targets specifically the under-resolved areas, whereas one based on the discretization error targets the under-resolved areas and the zones downstream of them [42, 41]. This makes the truncation error more suitable for adaptation purposes than the discretization error. Finally, it has been shown that controlling the truncation error targets the numerical accuracy of all functionals at once [18], ensuring that adapting a mesh using the truncation error leads necessarily to an error decrease in any other functional (e.g. lift or drag). For all these reasons, we focus on truncation error estimators in this paper.

From a practical point of view, the truncation error can be estimated using a hierarchy of meshes. On the one hand, Venditti and Darmofal [46] and Phillips et al. [32, 29] studied the possibility of estimating the truncation error by evaluating a coarse grid solution in the partial differential operator of a fine grid, an approach known as the coarse-to-fine approach. On the other hand, the fine-to-coarse approach, also known as the τ -estimation method, was introduced by Brandt [3] and consists in estimating the local truncation error by using a fine grid solution interpolated to the coarse grid. Phillips [30] showed that the fine-to-coarse (τ -estimation) method produces more accurate results than the coarse-to-fine approach and, therefore, it is the one retained in this work.

The τ -estimation approach has been successfully used for adaptation purposes in low-order Finite Difference [2] and Finite Volume schemes [13, 43, 44]. Moreover, Rubio et al. extended it to high-order methods using a continuous Chebyshev collocation method [40] and later the Discontinuous Galerkin Spectral Element Method (DGSEM) [41]. In that work, they studied the *quasi-a priori* truncation error estimation, which allows estimating the truncation error without having fully converged fine solutions, and introduced the concept of *isolated* truncation error (valid only for DG formulations), which only considers inner elemental contributions to the error and neglects the upwind contributions. More recently, Kompenhans et al. [18] applied these estimators to perform p-anisotropic adaptation for the Euler and Navier-Stokes equations, and compared τ -based to featured based adaption, showing better performance for the former [19]. The adaptation strategy consisted in converging a high order representation (reference mesh) to a specified global

residual and then performing a single error estimation followed by a corresponding p-adaptation process. Even though their methodology is very promising, we will show that it produces a large underestimation of the error for polynomial orders that are higher than the ones in the original reference mesh. This fact makes necessary to compute the initial solution in a very refined reference mesh to avoid inaccuracies.

In this paper, we extend the work on high-order τ -estimators by Rubio et al. [40, 41, 42], and formulate a new anisotropic truncation error estimator that exploits the tensor product basis expansion of the DGSEM. The new error estimator is shown to be suitable for performing anisotropic p-adaptation, and to have two main advantages over existing truncation error estimators; first, that it requires fewer operations to estimate the truncation error of all possible combinations of polynomial orders; and second, that it yields more accurate estimations of the truncation error for representations of a higher order than the reference mesh. This feature allows using reference meshes of a lower polynomial order, hence reducing the computational cost. We also analyze the properties of the traditional *non-isolated* truncation error and the *isolated* truncation error. To the authors' knowledge, this is the first time that a high-order truncation error estimator based on the τ -estimation method is formulated in an anisotropic/decoupled way, analyzed and tested.

The paper is organized as follows. In section 2, we present the mathematical background. First, the Discontinuous Galerkin Spectral Element Method is briefly summarized; then, we detail the existing techniques for approximating the truncation error of isotropic and anisotropic representations using the τ -estimation method. In section 3, the proposed anisotropic τ -estimator is introduced and analyzed. In section 4, we present a validation of the assumptions needed for formulating the new approach and study the properties of the proposed method by means of a manufactured solutions test case of the compressible Navier-Stokes equations. Finally, the conclusions are summarized in section 5.

2 Mathematical background

In section 2.1, we describe briefly the DGSEM approach. Section 2.2 contains the error definitions that will be used throughout the paper and provides an insight into the convergence properties of the different error measures. In section 2.3, we review the τ -estimation method for DGSEM schemes, and then we explain in section 2.4 how it has been used in the literature for obtaining anisotropic error extrapolations.

2.1 The Discontinuous Galerkin Spectral Element Method (DGSEM)

We consider the approximation of systems of conservation laws,

$$\mathbf{q}_t + \nabla \cdot \mathcal{F} = \mathbf{s}, \quad (2)$$

where \mathbf{q} is the vector of conserved variables, \mathcal{F} is the flux dyadic tensor which depends on \mathbf{q} , and \mathbf{s} is a source term. This system represents, among others, the compressible Navier-Stokes equations, as detailed in Appendix C. Multiplying equation 2 by a test function \mathbf{v} and integrating by parts over the domain Ω yields the weak formulation:

$$\int_{\Omega} \mathbf{q}_t \mathbf{v} d\Omega - \int_{\Omega} \mathcal{F} \cdot \nabla \mathbf{v} d\Omega + \int_{\partial\Omega} \mathcal{F} \cdot \mathbf{n} \mathbf{v} d\sigma = \int_{\Omega} \mathbf{s} \mathbf{v} d\Omega, \quad (3)$$

where \mathbf{n} is the normal unit vector on the boundary $\partial\Omega$. Let the domain Ω be approximated by a tessellation $\mathcal{T} = \{e\}$, a combination of K finite elements e of domain Ω^e and boundary $\partial\Omega^e$. Moreover, let \mathbf{q} , \mathbf{s} , \mathcal{F} and \mathbf{v} be approximated by piece-wise polynomial functions (that are continuous in each element) defined in the space of L^2 functions

$$\mathcal{V}^N = \{\mathbf{v}^N \in L^2(\Omega) : \mathbf{v}^N|_{\Omega^e} \in \mathcal{P}^N(\Omega^e) \ \forall \Omega^e \in \mathcal{T}\}, \quad (4)$$

where $\mathcal{P}^N(\Omega^e)$ is the space of polynomials of degree at most N defined in the domain of the element e . Remark that the functions in \mathcal{V}^N may be discontinuous at element interfaces and that the polynomial order N may be different from element to element. Equation 3 can then be rewritten for each element as:

$$\int_{\Omega^e} \mathbf{q}_t^{eN} \mathbf{v}^{eN} d\Omega^e - \int_{\Omega^e} \mathcal{F}^{eN} \cdot \nabla \mathbf{v}^{eN} d\Omega^e + \int_{\partial\Omega^e} \mathcal{F}^* \left(\mathbf{q}^{eN}, \mathbf{q}^{-N}, \mathbf{n} \right) \mathbf{v}^{eN} d\sigma^e = \int_{\Omega^e} \mathbf{s}^{eN} \mathbf{v}^{eN} d\Omega^e, \quad (5)$$

where the superindex “ e ” refers to the functions as evaluated inside the element e , i.e. $\mathbf{q}^{eN} = \mathbf{q}^N|_{\Omega^e}$; whereas the superindex “ $-$ ” refers to the value of the functions on the external side of the interface $\partial\Omega^e$. The numerical flux function, \mathcal{F}^* , allows to uniquely define the flux at the element interfaces and to weakly prescribe the boundary data as a function of the conserved variable on both sides of the boundary/interface (\mathbf{q}^{eN} and \mathbf{q}^{-N}) and the normal vector (\mathbf{n}). Multiple choices for the numerical flux functions can be found in the literature [45]. In the present work, we use Roe [38] as the advective Riemann Solver and Bassi-Rebay 1 [10] as the diffusive Riemann solver. Remark that the numerical flux must be computed in a specific manner when the representation is non-conforming [22].

Since \mathbf{q}^N , \mathbf{s}^N , \mathbf{v}^N and \mathcal{F}^N belong to the polynomial space \mathcal{V}^N , it is possible to express them inside every element as a linear combination of basis functions $\phi_n \in \mathcal{P}^N(\Omega^e)$,

$$\begin{aligned} \mathbf{q}|_{\Omega^e} &\approx \mathbf{q}^{eN} = \sum_n \mathbf{Q}_n^e \phi_n^e(\mathbf{x}), & \mathbf{s}|_{\Omega^e} &\approx \mathbf{s}^{eN} = \sum_n \mathbf{S}_n^e \phi_n^e(\mathbf{x}), \\ \mathbf{v}|_{\Omega^e} &\approx \mathbf{v}^{eN} = \sum_n \mathbf{V}_n^e \phi_n^e(\mathbf{x}), & \mathcal{F}|_{\Omega^e} &\approx \mathcal{F}^{eN} = \sum_n \mathcal{F}_n^e \phi_n^e(\mathbf{x}). \end{aligned} \quad (6)$$

Therefore, equation 5 can be expressed in a discrete form as

$$[\mathbf{M}]^e \frac{\partial \mathbf{Q}^e}{\partial t} + \mathbf{F}^e(\mathbf{Q}) = [\mathbf{M}]^e \mathbf{S}^e, \quad (7)$$

where $\mathbf{Q}^e = (\mathbf{Q}_1^e, \mathbf{Q}_2^e, \dots, \mathbf{Q}_n^e, \dots)^T$ is the local solution that contains the coefficients of the linear combination for the element e ; $\mathbf{Q} = (\mathbf{Q}^1, \mathbf{Q}^2, \dots, \mathbf{Q}^K)^T$ is the global solution that contains the information of all elements; $[\mathbf{M}]^e$ is known as the elemental mass matrix, and $\mathbf{F}^e(\cdot)$ is a nonlinear spatial discrete operator on the element level:

$$[\mathbf{M}]_{i,j}^e = \int_{\Omega^e} \phi_i^e \phi_j^e d\Omega^e \quad (8)$$

$$\mathbf{F}^e(\mathbf{Q})_j = \sum_i \left[- \int_{\Omega^e} \mathcal{F}_i^e \cdot \phi_i^e \nabla \phi_j^e d\Omega^e \right] + \int_{\partial\Omega^e} \mathcal{F}^{*N}(\mathbf{Q}^e, \mathbf{Q}^-, \mathbf{n}) \phi_j^e d\sigma^e. \quad (9)$$

Note that the operator \mathbf{F}^e is applied on the global solution, since it is the responsible for connecting the elements of the mesh (weakly). Assembling the contributions of all elements into the global system we obtain:

$$[\mathbf{M}] \frac{\partial \mathbf{Q}}{\partial t} + \mathbf{F}(\mathbf{Q}) = [\mathbf{M}] \mathbf{S}. \quad (10)$$

In the DGSEM [20], the tessellation is performed with non-overlapping hexahedral elements of order $N = (N_1, N_2, N_3)$ (independent in every direction) and the integrals are evaluated numerically by means of a Gaussian quadrature that is also of order $N = (N_1, N_2, N_3)$. For complex geometries, it is most convenient to perform the numerical integration in a reference element and transform the results to the physical space by means of a high-order mapping:

$$\mathbf{x}^e = \mathbf{x}^e(\boldsymbol{\xi}), \quad \boldsymbol{\xi} = (\xi, \eta, \zeta) \in [-1, 1]^3, \quad (11)$$

where the order of x_i^e is at most N_i^e (subparametric or at most isoparametric mapping). The differential operators can be expressed in the reference element in terms of the covariant (\mathbf{a}_i) and contravariant (\mathbf{a}^i) metric tensors:

$$\mathbf{a}_i = \frac{\partial \mathbf{x}^e}{\partial \xi_i}, \quad \mathbf{a}^i = \nabla \xi_i, \quad i = 1, 2, 3. \quad (12)$$

Under these mappings, the gradient and divergence operators become:

$$\nabla q = \frac{1}{J} \sum_{i=1}^d \frac{\partial}{\partial \xi_i} (J \mathbf{a}^i q), \quad \nabla \cdot \mathbf{f} = \frac{1}{J} \sum_{i=1}^d \frac{\partial}{\partial \xi_i} (J \mathbf{a}^i \cdot \mathbf{f}), \quad (13)$$

where the Jacobian of the transformation can be expressed in terms of the covariant metric tensor:

$$J = \mathbf{a}_i \cdot (\mathbf{a}_j \times \mathbf{a}_k), \quad (i, j, k) \text{ cyclic}. \quad (14)$$

For details on how to compute the metric terms for 2D and 3D geometries, see [21]. Furthermore, in the DGSEM the polynomial basis functions (ϕ_n in equation 6) are tensor product reconstructions of Lagrange interpolating polynomials on quadrature points in each of the Cartesian directions of the reference element:

$$\mathbf{q}^N = \sum_n \mathbf{Q}_n \phi_n(\mathbf{x}) = \sum_{i=0}^{N_1} \sum_{j=0}^{N_2} \sum_{k=0}^{N_3} \mathbf{Q}_{i,j,k} l_i(\xi) l_j(\eta) l_k(\zeta). \quad (15)$$

Therefore, $\mathbf{Q}_n = \mathbf{Q}_{i,j,k}$ are simply the nodal values of the solution, and $[\mathbf{M}]$ is a diagonal matrix containing the quadrature weights and the mapping terms. In the present work, we make use of the Legendre-Gauss quadrature points [20].

2.2 Definition of Errors

In this section, we define some measures of the error that will be used throughout the paper.

Definition 1 (Interpolation error) *The difference between a function and its polynomial interpolant of order N :*

$$\varepsilon_{\mathbf{q}}^N = \mathbf{q} - \mathbf{I}^N \mathbf{q}, \quad (16)$$

where $\mathbf{I}^N \mathbf{q}$ is the function that can be reconstructed using the polynomial expansion with coefficients \mathbf{Q}_i (equation 6). For sufficiently smooth functions, in the asymptotic range the interpolation error in an element e behaves as:

$$\left\| \varepsilon_{\mathbf{q}}^N |_{\Omega^e} \right\| \leq C_0^e e^{-N^e \eta_0^e}, \quad (17)$$

where C_0^e and η_0^e are constants that depend on the local smoothness of the function \mathbf{q} [4, 17] and N^e is the local polynomial order in the element e . In the DGSEM, the use of tensor-product bases in d dimensions allows decoupling the interpolation error in directional components, each of which depends solely on the polynomial order in the corresponding direction:

$$\varepsilon_{\mathbf{q}}^N = \sum_{i=1}^d \varepsilon_{\mathbf{q},i}^N \quad \text{such that} \quad \varepsilon_i = \varepsilon_i(N_i). \quad (18)$$

As a consequence, in the p-anisotropic DGSEM, the interpolation error exhibits a tensor-product-type error bound in d dimensions inside every element [41],

$$\left\| \varepsilon_{\mathbf{q}}^N |_{\Omega^e} \right\| \leq \sum_{i=1}^d C_{0,i}^e e^{-N_i^e \eta_{0,i}^e}. \quad (19)$$

Definition 2 (Discretization error) *The difference between the exact solution to the problem, $\bar{\mathbf{q}}$, and the one obtained with a discretization of order N , $\bar{\mathbf{q}}^N$:*

$$\epsilon^N = \bar{\mathbf{q}} - \bar{\mathbf{q}}^N. \quad (20)$$

The discretization error in an element is influenced by other elements because of the advection properties of the PDE. In fact, we will decouple the discretization error in *locally-generated* and *externally-generated* contributions for every element:

$$\epsilon^N |_{\Omega^e} = \epsilon_{\Omega^e}^N + \epsilon_{\partial\Omega^e}^N. \quad (21)$$

In the p-isotropic DGSEM, it can be assumed that the discretization error in each element behaves as [41, 42]:

$$\left\| \epsilon^N |_{\Omega^e} \right\| \leq C_\epsilon^e e^{-N^e \eta_\epsilon^e} + \sum_{\substack{k=1 \\ k \neq e}}^K C_\epsilon^{*k} e^{-N^k \eta_\epsilon^{*k}}, \quad (22)$$

where K is the number of elements, C_ϵ^e and η_ϵ^e are constants that depend on the smoothness of the solution in the element e [4, 17], and C_ϵ^{*k} and η_ϵ^{*k} are constants that depend both on the smoothness of the solution and the advection properties of the PDE. The first term on the right-hand side corresponds to the bound of the *locally-generated* discretization error (ϵ_Ω^N), whereas the second term is the bound of the *externally-generated* discretization error ($\epsilon_{\partial\Omega}^N$) which gathers the errors that are introduced through the Riemann solver. Note that ϵ^N is the minimum possible (lower bound of) ϵ^N . For an anisotropic representation in d dimensions, the expression becomes [41, 42, 14]:

$$\left\| \epsilon^N |_{\Omega^e} \right\| \leq \sum_{i=1}^d C_{\epsilon,i}^e e^{-N_i^e \eta_{\epsilon,i}^e} + \sum_{\substack{k=1 \\ k \neq e}}^K \sum_{i=1}^d C_{\epsilon,i}^k e^{-N_i^k \eta_{\epsilon,i}^k}. \quad (23)$$

Definition 3 (Quadrature error) *The quadrature error, also referred to as the numerical integration error, is the difference between the exact integral of a function and its approximation by a Gaussian quadrature:*

$$e_J^N = \int_{\Omega} q d\Omega - \int_{\Omega}^N q d\Omega, \quad (24)$$

where the superindex N on the integral indicates that it is approximated using a Gaussian quadrature of order N ,

$$\int_{\Omega}^N q d\Omega = \sum_{j=0}^N q_j w_j, \quad (25)$$

and w_j are the quadrature weights.

Definition 4 (Non-isolated truncation error) *We define the non-isolated truncation error of a discretization of order N as the difference between the discrete partial differential operator of order N and the exact partial differential operator applied to the exact solution:*

$$\tau^N = \mathcal{R}^N(\mathbf{I}^N \bar{\mathbf{q}}) - \mathcal{R}(\bar{\mathbf{q}}). \quad (26)$$

The exact partial differential operator can be derived from equation 2 as

$$\mathcal{R}(\mathbf{q}) = \mathbf{s} - \nabla \cdot \mathcal{F} = \mathbf{q}_t, \quad (27)$$

and the discrete partial differential operator is derived from equation 10 as

$$\mathcal{R}^N(\mathbf{I}^N \mathbf{q}) = [\mathbf{M}]\mathbf{S} - \mathbf{F}(\mathbf{I}^N \mathbf{q}), \quad (28)$$

where \mathcal{R}^N contains the sampled values of \mathcal{R}^N in all the nodes of the domain and \mathbf{I}^N is a sampling operator. \mathcal{R}^N is reconstructed from \mathcal{R}^N element-wise with

equation 6. Since for steady state, $\mathcal{R}(\bar{\mathbf{q}}) = 0$, the *non-isolated* truncation error can be then computed inserting equation 28 into 26 as

$$\boldsymbol{\tau}^N = \mathcal{R}^N(\mathbf{I}^N \bar{\mathbf{q}}) = [\mathbf{M}]\mathbf{S} - \mathbf{F}(\mathbf{I}^N \bar{\mathbf{q}}). \quad (29)$$

The dependence of the *non-isolated* truncation error on the discretization error is obtained by using definition 2 and expanding equation 29 as a Taylor series:

$$\boldsymbol{\tau}^N = \left. \frac{\partial \mathcal{R}^N}{\partial \mathbf{Q}^N} \right|_{\bar{\mathbf{Q}}^N} \boldsymbol{\epsilon}^N + \mathcal{O}((\boldsymbol{\epsilon}^N)^2). \quad (30)$$

Taking into account equations 30 and 23, and based on previous numerical results [42, 41], Kompenhans et al. [18] stated that the truncation error in an element is bounded by

$$\left\| \boldsymbol{\tau}^N \Big|_{\Omega^e} \right\| \leq \sum_{i=1}^d C_i^e e^{-N_i^e \eta_i^e} + \|\boldsymbol{\tau}_{\partial\Omega^e}\|. \quad (31)$$

This expression was validated experimentally [18, 19]. The first term in equation 31 is the bound of the *locally-generated* truncation error, whereas the second term is the bound of the *externally-generated* truncation error that enters through the Riemann solver and does not depend on the local polynomial orders. The second term is a consequence of the dependence of the discretization error on the solution in other elements.

Definition 5 (Isolated truncation error) *The isolated truncation error is defined as [41]*

$$\hat{\boldsymbol{\tau}}^N = \hat{\mathcal{R}}^N(\mathbf{I}^N \bar{\mathbf{q}}), \quad (32)$$

where $\hat{\mathcal{R}}^N(\cdot)$ is the *isolated* discrete partial differential operator, which is derived in the same manner as $\mathcal{R}^N(\cdot)$, but \mathcal{F} is not substituted by \mathcal{F}^* during the process (equation 5). Therefore, the sampled form of the discrete isolated partial differential operator yields

$$\hat{\boldsymbol{\tau}}^N = \hat{\mathcal{R}}^N(\mathbf{I}^N \bar{\mathbf{q}}) = [\mathbf{M}]\mathbf{S} - \hat{\mathbf{F}}(\mathbf{I}^N \bar{\mathbf{q}}), \quad (33)$$

where the elemental contribution to the nonlinear discrete operator is

$$\hat{\mathbf{F}}^e(\mathbf{Q}^e)_j = \sum_i \left[- \int_{\Omega^e} \mathcal{F}_i \cdot \phi_i^e \nabla \phi_j^e d\Omega^e \right] + \int_{\partial\Omega^e} \mathcal{F}^N \cdot \mathbf{n} \phi_j^e d\sigma^e. \quad (34)$$

This change eliminates the influence of the neighboring elements and boundaries in the truncation error of each element. The dependence of the *isolated* truncation error on the interpolation error of the fluxes inside an element ($\varepsilon_{\mathcal{F},e}^N$) can be expressed as (see Appendix A and [41]):

$$\hat{\boldsymbol{\tau}}^N \Big|_{\Omega^e} \approx \left(\nabla \cdot \varepsilon_{\mathcal{F}}^N \Big|_{\Omega^e}, \phi \right)_{\Omega^e}^N. \quad (35)$$

This shows that $\hat{\boldsymbol{\tau}}$ indeed depends only on the discrete representation of the numerical solution in the element e . Rubio et al. [41] pointed out that the *isolated* truncation error might be a better sensor for adaptation algorithms for hyperbolic PDEs than its *non-isolated* counterpart or the discretization error, since unlike

the last two, the first one is not affected by neighbors' errors. Notice that equation 35 resembles the DETE [39]. In this case, the isolated truncation error acts as a source term for the interpolation error. In consequence, decreasing the *isolated* truncation error reduces the interpolation error.

Finally, it is important to note that the spectral convergence of the *isolated* truncation error is similar to the *non-isolated* truncation error [41, 42] and can be expressed as

$$\left\| \hat{\tau}_e^N |_{\Omega^e} \right\| \leq \sum_{i=1}^d C_i^e e^{-N_i^e \eta_i^e}. \quad (36)$$

Remark that, because of the reasons exposed above, in this case there is no *externally-generated* truncation error. The *hat notation* will be dropped from now on since, unless explicitly stated, the formulations in this paper are valid for both the *non-isolated* and the *isolated* truncation errors.

2.3 τ -Estimation method

Since in general the exact solution to the problem is not available, we are interested in using an estimation for equations 29 and 33. The τ -estimation method makes use of an approximate solution on a reference mesh of order $P > N$ instead of the exact one. The most straightforward methodology is to converge this high-order solution to a low residual near machine round-off, $\tilde{\mathbf{Q}}^P$. This is known as the *a posteriori* approach. In practice, one can also use a non-converged solution, $\tilde{\mathbf{Q}}^P$. This is known as the *quasi-a priori* approach. In this paper, we use the following formulation, which is valid for the *a-posteriori* method and the *quasi a-priori* approach without correction:

$$\tau_P^N = \mathcal{R}^N(\mathbf{I}_P^N \mathbf{Q}^P) = [\mathbf{M}^N] \mathbf{S}^N - \mathbf{F}^N(\tilde{\mathbf{Q}}^P), \quad (37)$$

where \mathbf{I}_P^N is an interpolation operator from order P to order N . For compactness, the notation of this work omits the interpolation matrix such that $\mathcal{R}^N(\mathbf{Q}^P) = \mathcal{R}^N(\mathbf{I}_P^N \mathbf{Q}^P)$. Equation 37 is valid for both the *isolated* (inserting the *hats*) and the *non-isolated* truncation error. Note that the truncation error estimation can be easily performed for anisotropic polynomial representations of d dimensions. For instance, in a 2D anisotropic case, equation 37 can be rewritten as:

$$\tau_{P_1 P_2}^{N_1 N_2} = [\mathbf{M}^{N_1 N_2}] \mathbf{S}^{N_1 N_2} - \mathbf{F}^{N_1 N_2}(\tilde{\mathbf{Q}}^{P_1 P_2}). \quad (38)$$

2.4 Low order extrapolation of the truncation error estimations

In this section, we review the method proposed by Kompenhans et al. [18] to extrapolate the τ -estimations of anisotropic representations. This method was successfully used to perform a p-adaptation strategy [18, 19]. We will show that their strategy can be classified as a low order extrapolation. In order to do so, let us first introduce the concept of truncation error map.

Definition 6 (Truncation error map) *The (graphical) representation of the truncation error behavior inside an element with respect to the polynomial order as a $(d + 1)$ -dimensional plot of $\log \|\tau^N\|$ as a function of the polynomial order in every direction of the reference element $N = (N_1, \dots, N_d)$, where d is the number of dimensions.*

Because of the spectral convergence of the truncation error in the asymptotic range, the one-dimensional (or isotropic d -dimensional) map turns out to be a discrete scatter plot of points that describe a linear function with a negative slope (the convergence rate η), as shown in Figure 1(a).

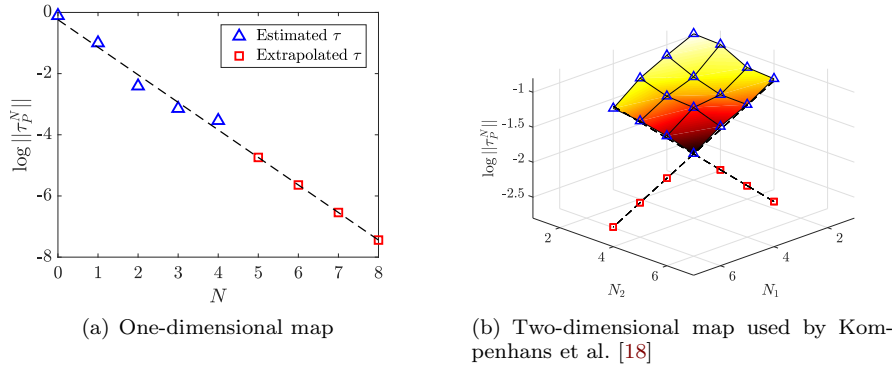


Fig. 1 One- and two-dimensional truncation error maps constructed with $P = 5$ showing estimated and extrapolated values for a toy problem (illustrative)

Kompenhans et al. [18] used the estimated truncation error map to adapt the polynomial orders of a given mesh using a specified maximum permitted error threshold, τ_{max} . The method for estimating the map consists of four steps:

1. Generate an *inner* map for $N_i < P_i$ using equation 38. This requires n_{eval} evaluations of the discrete partial differential operator \mathcal{R}^N , where

$$n_{eval} = \prod_{i=1}^d (P_i - 1). \quad (39)$$

The estimated points of the *inner* map are marked as blue triangles in Figure 1.

2. Use the *inner* map to look for a combination of polynomial orders that fulfills the specified error threshold. If a combination fulfills τ_{max} , adapt the polynomial order and exit the adaptation process. Otherwise, additional considerations are required.
3. Compute $\log \|\tau^{N_i N_j}\|$ and perform a linear regression analysis in the direction i in order to describe the behavior of $\log \|\tau\|$ as a function of N_i ($N_j = P_j - 1$). The result of the linear regression is marked with a dashed line in Figure 1.

4. Use the linear regression to estimate the truncation error for $N_i \geq P_i$, and select the value of N_1 and N_2 independently from these extrapolations. The extrapolated values of the truncation error are marked with red squares in Figure 1.

This procedure is performed for every element in all the Cartesian directions to adapt the mesh. For further details, refer to the original paper by Kompenhans et al. [18] and to our example in section 4.2.

2.4.1 Analysis of the method

Two remarks can be made about the described four-step procedure:

Remark 1 Steps 3 and 4 assume that the spectral convergence observed in 1D extends to higher dimensions along iso- N_i lines of the truncation error map.

Remark 2 For the non-isolated truncation error, the behavior shown in Figure 1 can only be expected for the locally-generated component (see equation 31). This means that the extrapolation procedure may predict unexpected behaviors if the truncation error in neighboring elements is high, i.e., if the τ -estimation procedure is not performed element-wise while keeping the polynomial order in other elements sufficiently¹ high.

As stated in the remark 1, the extrapolation procedure assumes that the truncation error decreases exponentially along iso- N_i lines of the truncation error map. That is the same as saying that the truncation error map is a plane for $d = 2$, and in general that it is a hyperplane of dimension $d + 1$. In Figure 2 we present an illustration that resembles the hyperplane behavior in two dimensions for perfect spectral convergence. The described methodology consists in constructing d iso- N_i lines on the hyperplane, which should contain the values of the truncation error for $N_j = P_j - 1 \forall N_i$ (red line with triangular markers and black line with circular markers in Figure 2). In that scenario, selecting N_i independently can be regarded as a conservative criterion, since in the hyperplane we have:

- In 2D:

$$\begin{aligned}\tau^{N_1 N_2} &\leq \tau^{P_1 N_2}, \\ \tau^{N_1 N_2} &\leq \tau^{N_1 P_2}.\end{aligned}$$

- In 3D:

$$\begin{aligned}\tau^{N_1 N_2 N_3} &\leq \tau^{P_1 N_2 N_3}, \\ \tau^{N_1 N_2 N_3} &\leq \tau^{N_1 P_2 N_3}, \\ \tau^{N_1 N_2 N_3} &\leq \tau^{N_1 N_2 P_3}.\end{aligned}$$

for $N_i \geq P_i$. See Figure 2.

¹ Sufficiently high does not necessarily mean that the polynomial order of the other elements must be kept in P , but that it must be high enough so that the *externally-generated* contributions to the truncation error are less than the *internally-generated* ones.

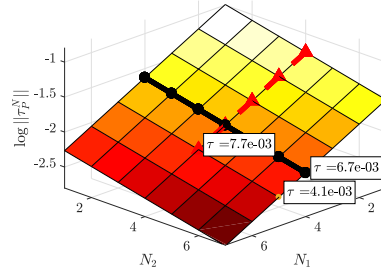


Fig. 2 Hyperplane behavior of the truncation error of a toy problem (illustrative)

Hereinafter, the method by Kompnans et al. shall be referred to as the *low order extrapolation method*, since it supposes that the truncation error map ($\log \|\tau\|$) has a linear behavior. In light of the analysis in section 3, we will be able to formulate a *high order extrapolation method* that provides extrapolated estimations with increased accuracy.

3 New anisotropic truncation error estimation

In this section, we present the new anisotropic truncation error estimator, discuss some of its properties and compare them with the error estimators that have been used in the literature for performing anisotropic p-adaptation. The formulation of this new estimator involved a mathematical proof based on specific assumptions that is detailed in section 3.1. In section 3.2, we analyze the convergence behavior of the anisotropic estimator. In section 3.3, we describe how the new estimator can be used for approximating the truncation error of higher-order representations, and prove that it is superior to existing τ -estimators at obtaining these approximations.

3.1 Anisotropic τ -estimation

The anisotropic τ -estimator is a generalization of the ideas reviewed in section 2.3 and is based on four assumptions that are explained first. For the sake of readability and without loss of generality, all the mathematical statements in this section are for 2D formulations, where $N = (N_\xi, N_\eta) = (N_1, N_2)$ are the polynomial orders in the 2 directions of the reference element. However, all the statements and proofs can be directly generalized to d dimensions.

Assumptions

Following assumptions are a consequence of the tensor product basis functions of the DGSEM and hold for sufficiently smooth solutions in the asymptotic range. The assumptions are:

- (a) The truncation error has an anisotropic behavior and, therefore, can be decoupled in its directional components:

$$\tau^{N_1 N_2} \approx \tau_1^{N_1 N_2} + \tau_2^{N_1 N_2}. \quad (40)$$

Here, it is important to note that τ_i is the projection of the global truncation error, τ , into the local direction, i .

- (b) The *locally-generated* truncation error in each direction depends only on the polynomial order in that direction:

$$\tau_{\Omega, i}^{N_1 N_2} \approx \tau_{\Omega, i}^{N_1 N_2}(N_i) \quad (41)$$

Assumptions (a) and (b) follow from the work of Rubio et al. [41, 42]. Furthermore, assumption (b) relates to the anisotropic spectral convergence behavior of the truncation error (equations 31 and 36).

Theorem 1 *The truncation error of a DGSEM discretization of order (N_1, N_2) can be approximated from a semi-converged solution of order (P_1, P_2) , such that $P_i > N_i$, as the sum of the directional τ -estimations obtained by coarsening in the different space dimensions:*

$$\tau^{N_1 N_2} \approx \tau_{P_1 P_2}^{N_1 P_2} + \tau_{P_1 P_2}^{P_1 N_2} \quad (42)$$

Proof.

This proof is specific for the *isolated* truncation error. We refer to Appendix B for a brief proof that Theorem 1 also holds for the *non-isolated* truncation error under additional assumptions.

Let us note that assumptions (a) and (b) are consistent with the dependence of the *isolated* truncation error on the interpolation error (equation 35) and the anisotropic behavior of the latter (equation 19).

We start by obtaining the analytical expression for the *isolated* τ -estimation. To that end, we use the same procedure as in Appendix A. The estimate of the *isolated* truncation error in the DGSEM can be expressed for any basis function ϕ in an element e as

$$\hat{\tau}_P^N|_{\Omega^e} = \hat{\mathcal{R}}(\mathbf{I}^N \bar{\mathbf{q}}^P) = \int_{\Omega^e} \mathbf{s}^N \phi d\Omega + \int_{\Omega^e} \mathcal{F}^N(\bar{\mathbf{q}}^P) \cdot \nabla \phi d\Omega - \int_{\partial\Omega^e} \mathcal{F}^N(\bar{\mathbf{q}}^P) \cdot \mathbf{n} \phi d\sigma, \quad (43)$$

In this case, instead of the exact solution to the problem, $\bar{\mathbf{q}}$, we use a solution on a higher order mesh, $\bar{\mathbf{q}}^P$. Therefore, using the definition of interpolation error (equation 16) and discretization error (equation 20), the flux is

$$\mathcal{F}^N = \mathbf{I}^N \mathcal{F}(\bar{\mathbf{q}}^P) = \mathcal{F}(\bar{\mathbf{q}}^P) - \varepsilon_{\mathcal{F}}^N = \mathcal{F}(\bar{\mathbf{q}}) + \left. \frac{\partial \mathcal{F}}{\partial \mathbf{q}} \right|_{\bar{\mathbf{q}}} \epsilon^P - \varepsilon_{\mathcal{F}}^N + \mathcal{O}((\epsilon^P)^2), \quad (44)$$

and the source term is

$$\mathbf{s}^N = \mathbf{I}^N \mathbf{s} = \mathbf{s} - \varepsilon_{\mathbf{s}}^N. \quad (45)$$

Inserting equations 44 and 45 into 43, and integrating by parts we obtain

$$\hat{\tau}_P^N \Big|_{\Omega^e} = \left(\nabla \cdot \varepsilon_{\mathcal{F}}^N, \phi \right)_{\Omega^e}^N + \left(\nabla \cdot \frac{\partial \mathcal{F}}{\partial \mathbf{q}} \Big|_{\bar{\mathbf{q}}} \varepsilon^P, \phi \right)_{\Omega^e}^N + \mathcal{O}((\varepsilon^P)^2) + \mathcal{O}(e_f^N). \quad (46)$$

Remark that although the *isolated* truncation error of an element does not depend on external sources, its approximation by τ -estimation is affected by the discretization error of the reference mesh, ε^P . This translates into a weak influence of external (upwind) errors transmitted through the Riemann solver. In the two-dimensional case and coarsening in only one direction (here the direction (1)), equation 46 becomes

$$\hat{\tau}_{P_1 P_2}^{N_1 P_2} \Big|_{\Omega^e} = \left(\nabla \cdot \varepsilon_{\mathcal{F}}^{N_1 P_2}, \phi \right)_{\Omega^e}^{N_1 P_2} + \left(\nabla \cdot \frac{\partial \mathcal{F}}{\partial \mathbf{q}} \Big|_{\bar{\mathbf{q}}} \varepsilon^{P_1 P_2}, \phi \right)_{\Omega^e}^{N_1 P_2} + \mathcal{O}((\varepsilon^{P_1 P_2})^2) + \mathcal{O}(e_f^{N_1 P_2}). \quad (47)$$

Now, we rewrite equation 47 decoupling the interpolation error in directional components and taking into account that $\varepsilon_2^{N_1 P_2} = \varepsilon_2^{P_1 P_2}$ (equation 18):

$$\hat{\tau}_{P_1 P_2}^{N_1 P_2} = \left(\nabla \cdot \varepsilon_{\mathcal{F},1}^{N_1 P_2}, \phi \right)_{\Omega^e}^{N_1 P_2} + \left(\nabla \cdot \varepsilon_{\mathcal{F},2}^{P_1 P_2}, \phi \right)_{\Omega^e}^{N_1 P_2} + \left(\nabla \cdot \frac{\partial \mathcal{F}}{\partial \mathbf{q}} \Big|_{\bar{\mathbf{q}}} \varepsilon^{P_1 P_2}, \phi \right)_{\Omega^e}^{N_1 P_2} + \mathcal{O}((\varepsilon^{P_1 P_2})^2) + \mathcal{O}(e_f^{N_1 P_2}). \quad (48)$$

Notice that all terms on the right-hand side, except for the first one and the quadrature error, are of the order of errors on the higher-order mesh. Therefore, and taking into account that we are coarsening in the direction (1), for sufficiently smooth solutions we can expect the first term on the right-hand side to be the leading term. Simplifying, the directional $\hat{\tau}$ -estimation provides

$$\hat{\tau}_{P_1 P_2}^{N_1 P_2} \approx \left(\nabla \cdot \varepsilon_{\mathcal{F},1}^{N_1 P_2}, \phi \right)_{\Omega^e}^{N_1 P_2}. \quad (49)$$

On the other hand, inserting equation 18 into 35, the *isolated* truncation error of a representation of order $N = (N_1, N_2)$ yields

$$\hat{\tau}^{N_1 N_2} \Big|_{\Omega^e} \approx \sum_{i=1}^d \left(\nabla \cdot \varepsilon_{\mathcal{F},i}^{N_1 N_2}, \phi \right)_{\Omega^e}^{N_1 N_2}. \quad (50)$$

Notice, again, that the directional components of the interpolation error only depend on the polynomial order in the corresponding direction (equation 18). Therefore, neglecting additional quadrature errors, we recover equation 42 for the *isolated* truncation error by combining equations 49 and 50:

$$\hat{\tau}^{N_1 N_2} \approx \hat{\tau}_{P_1 P_2}^{N_1 P_2} + \hat{\tau}_{P_1 P_2}^{P_1 N_2}. \quad (51)$$

□

From the previous analysis we can conclude that, when the τ -estimation method is performed coarsening only in the direction i , the result is an approximation to

the i -directional component of the truncation error, τ_i . We can also arrive at this conclusion intuitively if we realize that $\mathbf{Q}^{P_1 P_2}$ cannot be better than $\mathbf{Q}^{N_1 P_2}$ at describing the solution in the direction (2).

Theorem 1 can be easily generalized to three dimensions to obtain

$$\begin{aligned}\tau^{-N_1 N_2 N_3} &\approx \tau_1^{N_1 N_2 N_3} + \tau_2^{N_1 N_2 N_3} + \tau_3^{N_1 N_2 N_3} \\ \tau^{-N_1 N_2 N_3} &\approx \tau_{P_1 P_2 P_3}^{N_1 P_2 P_3} + \tau_{P_1 P_2 P_3}^{P_1 N_2 P_3} + \tau_{P_1 P_2 P_3}^{P_1 P_2 N_3}.\end{aligned}$$

3.2 Convergence behavior of the anisotropic truncation error

In this section we analyze the convergence properties of the truncation error map using Theorem 1. Let us first consider the directional components of the truncation error.

Theorem 2 *The directional components of the locally-generated truncation error exhibit spectral convergence with respect to the polynomial order in the corresponding direction:*

$$\|\tau_{\Omega^e, i}\| \leq C_i^e e^{-N_i^e \eta_i^e} \quad (52)$$

Proof. According to assumption (b) (equation 41), each directional component of the *locally-generated* truncation error, $\tau_{\Omega, i}$, depends solely on the polynomial order in the corresponding direction, N_i . If we insert equation 41 into equation 36 and analyze the dependencies term by term, we recover 52 for the *isolated* truncation error. In the same way, if we insert equation 41 into 31, we recover 52 for the *non-isolated* truncation error. \square

Now, we are able to analyze the convergence behavior along lines of the truncation error map, where a line in d dimensions is defined as:

$$a_1 N_1 + a_2 N_2 + \dots + a_d N_d = b, \quad (53)$$

with $a_i, b \in \mathbb{R}$.

Theorem 3 *The total truncation error does not necessarily decrease exponentially along lines of the truncation error map.*

Proof. The corresponding positive statement can be easily proven wrong with a counterexample. Let us consider a 2D anisotropic representation. From theorem 2, we know that the truncation error of each directional component in an element, τ_i^N , decreases exponentially when increasing N_i ; and that the decreasing rate is η_i , a constant that depends on the smoothness of the solution in the direction i . Let us suppose that for a certain element in a mesh, the directional components of the error have the same value for a specific combination of polynomial orders (\bar{N}_1, \bar{N}_2) in a certain norm:

$$\left\| \tau_1^{\bar{N}_1 \bar{N}_2} \right\| = \left\| \tau_2^{\bar{N}_1 \bar{N}_2} \right\| = C. \quad (54)$$

Let us analyze the convergence rate along an iso- N_i line of the truncation error map with constant $N_1 = \bar{N}_1$, i.e. the convergence rate of $\tau^{\bar{N}_1 N_2}$ as a function of N_2 . Note that, according to assumption (b), along the line we have

$$\begin{aligned} \tau_1^{\bar{N}_1 N_2} &\approx \tau_1^{\bar{N}_1 \bar{N}_2} \\ \left\| \tau_1^{\bar{N}_1 N_2} \right\| &\approx \left\| \tau_1^{\bar{N}_1 \bar{N}_2} \right\| = C. \end{aligned} \quad (55)$$

Furthermore, assumption (a) states that the total truncation error along the line of the map is:

$$\tau^{\bar{N}_1 N_2} \approx \tau_1^{\bar{N}_1 N_2} + \tau_2^{\bar{N}_1 N_2}. \quad (56)$$

Substituting equation 55 into 56 and using the triangle inequality yields:

$$\left\| \tau^{\bar{N}_1 N_2} \right\| \leq C + \left\| \tau_2^{\bar{N}_1 N_2} \right\|. \quad (57)$$

Remember that the truncation error map is defined as the dependence of $\log \left\| \tau^{N_1 N_2} \right\|$ on (N_1, N_2) (definition 6). Therefore, taking logarithms in both sides and rearranging, equation 57 can be rewritten in two equivalent forms:

$$i) \quad \log \left\| \tau^{\bar{N}_1 N_2} \right\| \leq \log \left\| \tau_2^{\bar{N}_1 N_2} \right\| + \log \left(1 + \frac{C}{\left\| \tau_2^{\bar{N}_1 N_2} \right\|} \right), \quad (58)$$

$$ii) \quad \log \left\| \tau^{\bar{N}_1 N_2} \right\| \leq \log(C) + \log \left(1 + \frac{\left\| \tau_2^{\bar{N}_1 N_2} \right\|}{C} \right). \quad (59)$$

For $N_2 \ll \bar{N}_2$, the second term on the right-hand side of equation 58 vanishes, which indicates that the convergence rate of the truncation error along an iso- N_i line of constant $N_1 = \bar{N}_1$ tends to η_2 . On the other hand, for $N_2 \gg \bar{N}_2$, the second term on the right-hand side of equation 59 vanishes, which implies that the convergence rate along an iso- N_i line of constant $N_1 = \bar{N}_1$ tends to zero, since the truncation error is bounded by $\log(C)$, a constant that does not depend on N_2 . In other words, the iso- N_i line on the hyperplane for $N_1 = \bar{N}_1$ is not a straight line. \square

3.3 High order extrapolation of the truncation error estimations

In this section, we present a procedure for extrapolating the truncation error estimations (*inner* map) that can be obtained by applying Theorem 1. Since Theorem 3 rules out the possibility of extrapolating along iso- N_i lines of the truncation error map, we take advantage of the anisotropic behavior of the truncation error (equation 40) and the spectral convergence of its directional components (Theorem 2). The proposed methodology, which is valid for both the *isolated* and *non-isolated* truncation error, can be summarized in three steps:

1. Perform anisotropic coarsening to obtain τ_i (Theorem 1) and construct the *inner* truncation error map directly. In d dimensions, this requires only n_{eval}^{new} evaluations of the discrete partial differential operator \mathcal{R}^N , where

$$n_{eval}^{new} = \sum_{i=1}^d (P_i - 1). \quad (60)$$

2. Compute $\log \|\tau_i\|$ and perform a linear regression analysis in the direction i in order to describe the behavior of $\log \|\tau_i\|$ as a function of N_i . This is supported on the proved spectral behavior of the directional components of the truncation error (Theorem 2).
3. Construct the *outer* truncation error map using equation 42 and the extrapolated values of $\log \|\tau_i\|$:

$$\log \|\tau\| = \log \left\| \sum_{i=1}^d \tau_i \right\|. \quad (61)$$

An example is provided in section 4.

3.4 Theoretical comparison of the new anisotropic τ -estimation with previous approaches

Figure 3(a) illustrates the theoretically predicted behavior of the truncation error map that is obtained with the new anisotropic τ -estimation method for a toy problem (only illustrative). As noted in the proof of Theorem 3, remark that along an iso- N_i line, the truncation error firstly decays exponentially for low $N_{j \neq i}$ and then tends asymptotically to a constant value for high $N_{j \neq i}$. As can be seen, contrary to the *low-order extrapolation*, the new anisotropic τ -estimation does not assume that the truncation error map has a linear behavior. That is the reason why it is called *high-order extrapolation*. Figure 3(b) shows a comparison of the hyperplane behavior with the one obtained using the new anisotropic τ -estimation method. As can be seen, the hyperplane tends to underpredict the truncation error for some combinations of polynomial orders as compared to the new truncation error estimator. A comparison of the output of both estimation methods with the exact truncation error in a test case is provided in section 4.2.

It is noteworthy that even though the method of Kompenhans et al. [18] supposes hyperplane behavior, their strategy of selecting the polynomial order in every direction independently minimizes the error involved in the *low order extrapolation* (compare the values of τ in Figures 3(a) and 2). Furthermore, remark that for $N_1 \gg N_2$ and $N_2 \gg N_1$ the new anisotropic estimation tends to have a hyperplane behavior. In fact, Kompenhans et al. [18, section 5.1] state that only the values of the truncation error where $N_1 \gg N_2$ or $N_2 \gg N_1$ should be used for the least square fitting. The high-order extrapolation can be seen as a form of bypassing this requirement.

Table 1 provides a final summary comparing the new estimation method and the previous methodology by Kompenhans et al. [18].

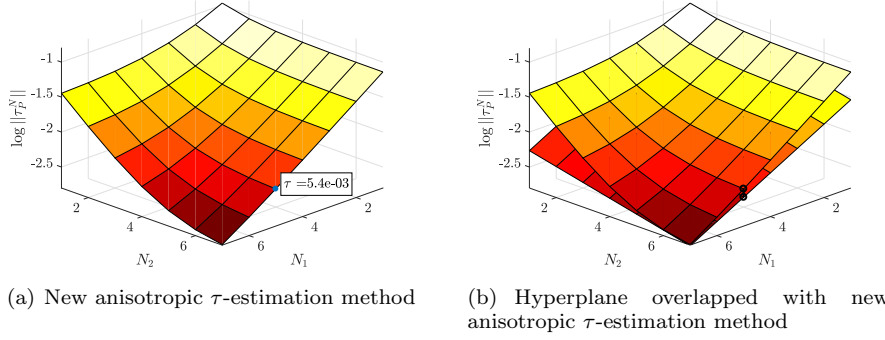


Fig. 3 Spatial representation of two-dimensional anisotropic truncation error maps: behavior predicted by the new anisotropic τ -estimation method (a), hyperplane behavior (Figure 2) overlapped with the values predicted by the new anisotropic τ -estimation method (b)

Table 1 Comparison of anisotropic τ -estimation methods in d dimensions performed with a reference mesh of order (P_1, \dots, P_d) . \mathcal{R}^N is the discrete partial differential operator.

Feature	Kompenhans et al. [18]	Proposed τ -estimation
Number of evaluations of \mathcal{R}^N for inner map	$\prod_{i=1}^d (P_i - 1)$	$\sum_{i=1}^d (P_i - 1)$
Accuracy of inner map	Very good	Good
Accuracy of outer map	Poor	Good

4 Validation of the anisotropic τ -estimation method

The compressible Navier-Stokes equations can be written in conservative form (see Appendix C) and discretized using the DGSEM, as explained in section 2.1. In order to test the accuracy of the proposed τ -estimation method, a 2D manufactured solutions test case is analyzed. The exact solution selected for the problem is

$$\begin{aligned} \rho &= p = e^{-5(4(x-\frac{1}{2})^2 + (y-\frac{1}{2})^2)} + 1, \\ u &= v = 1, \end{aligned} \quad (62)$$

which is simulated in the unit square, as depicted in Figure 4. Inserting equation 62 into 81, the source term for the 2D compressible Navier-Stokes equations yields

$$\mathbf{s} = \begin{bmatrix} s_\rho \\ s_{\rho u} \\ s_{\rho v} \\ s_{\rho e} \end{bmatrix} = \begin{bmatrix} 40(x - \frac{1}{2}) + 10(y - \frac{1}{2}) \\ 80(x - \frac{1}{2}) + 10(y - \frac{1}{2}) \\ 40(x - \frac{1}{2}) + 20(y - \frac{1}{2}) \\ [40(x - \frac{1}{2}) + 10(y - \frac{1}{2})] [\frac{1}{\gamma-1} + 2] \end{bmatrix} e^{5(4(x-\frac{1}{2})^2 + (y-\frac{1}{2})^2)}. \quad (63)$$

The main interest is to validate the proposed error estimator and compare its outcome with previous works. Since the method of Kompenhans et al. [18] explained in section 2.4 was formulated and used with the *non-isolated* truncation

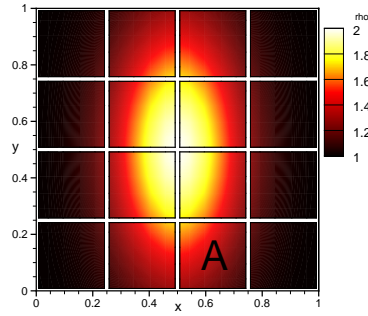


Fig. 4 Density (ρ) contours for the proposed manufactured solutions test case

error, the results that are shown in sections 4.1 and 4.2 were obtained for the *non-isolated* truncation error estimator (τ_P^N). However, similar results can be obtained for the *isolated* truncation error, since its maps exhibit the same behavior as the ones presented here. In addition, in section 4.3 we compare the truncation error estimator with the *isolated* truncation error estimator when used for driving a p-adaptation procedure.

4.1 Truncation error maps and number of degrees of freedom

A fully time-converged solution ($\|\mathcal{R}^P\|_\infty < 10^{-10}$) of order 5 ($P = P_1 = P_2 = 5$) is used to estimate the truncation error using the method of section 3.1. The results for element *A* are depicted in Figure 5(a). Figure 5(b) shows the exact truncation error. It can be seen that the proposed method predicts a truncation error map that is very similar to the exact one, even for extrapolated values. Hence, in agreement with the obtained results, the assumptions of section 3.1 are reasonable. These maps can be used for selecting an appropriate combination of polynomial orders such that a maximum truncation error τ_{max} is achieved employing a minimum number of degrees of freedom.

Figure 6 shows the map of the number degrees of freedom (DOFs) for every (N_1, N_2) -combination. The polynomial orders that achieve a truncation error $\tau < \tau_{max}$ are marked with black squares. Let us remark that, although these results are not exactly the same for the estimated and exact truncation error maps, they are very similar. Therefore, we conclude that the proposed estimation method may be used for adaptation purposes. Notice that there are many alternatives that produce a truncation error in the desired range, but there is only one that minimizes the number of degrees of freedom and, therefore, the computational cost.

4.2 Comparison with previous methodologies

Figure 7 shows the 3D representation of the exact truncation error map (a), the one obtained with the *high-order extrapolation* (b), and the one obtained with the

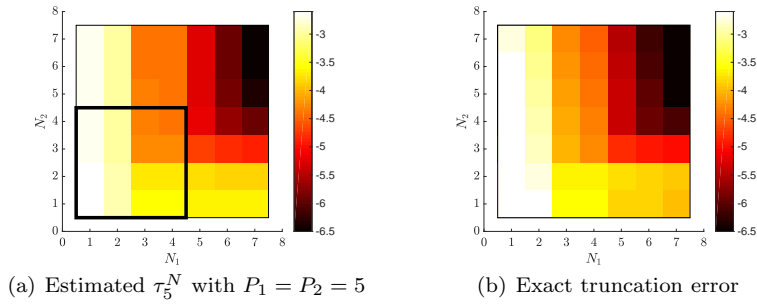


Fig. 5 Truncation error estimation (a) and exact values (b) for different polynomial order combinations in element A (logarithmic scale). Outside the black box (a) are the extrapolated values of the estimated truncation error

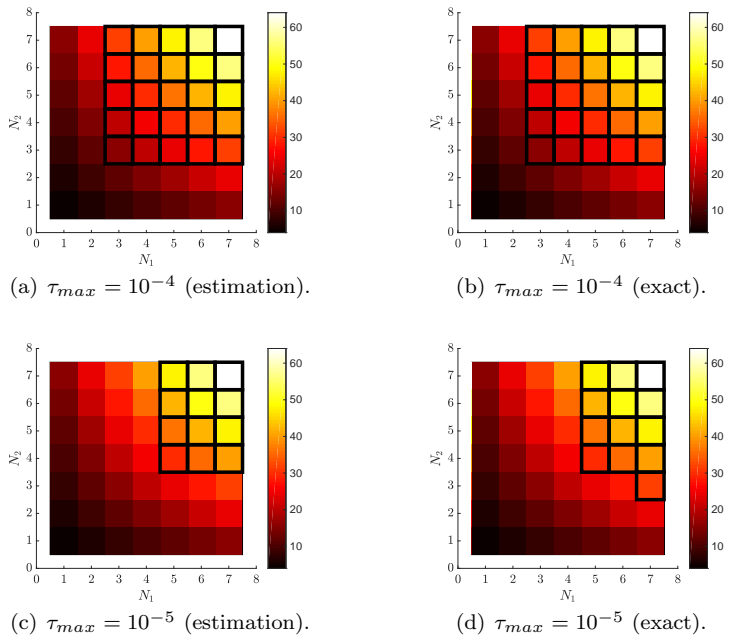


Fig. 6 Contour of the number of degrees of freedom for every polynomial order considered for performing p-adaptation. The combinations (N_1, N_2) that fulfill the τ_{max} threshold are marked with black squares

low-order extrapolation (c) -here, we illustrate the complete hyperplane. The maps were generated with the same fully time-converged solution of order $P_1 = P_2 = 5$. As can be seen, the truncation error map generated with the *high-order extrapolation* bears close resemblance to the exact one, whereas the hyperplane underpredicts the truncation error in some regions, as anticipated in section 3.4.

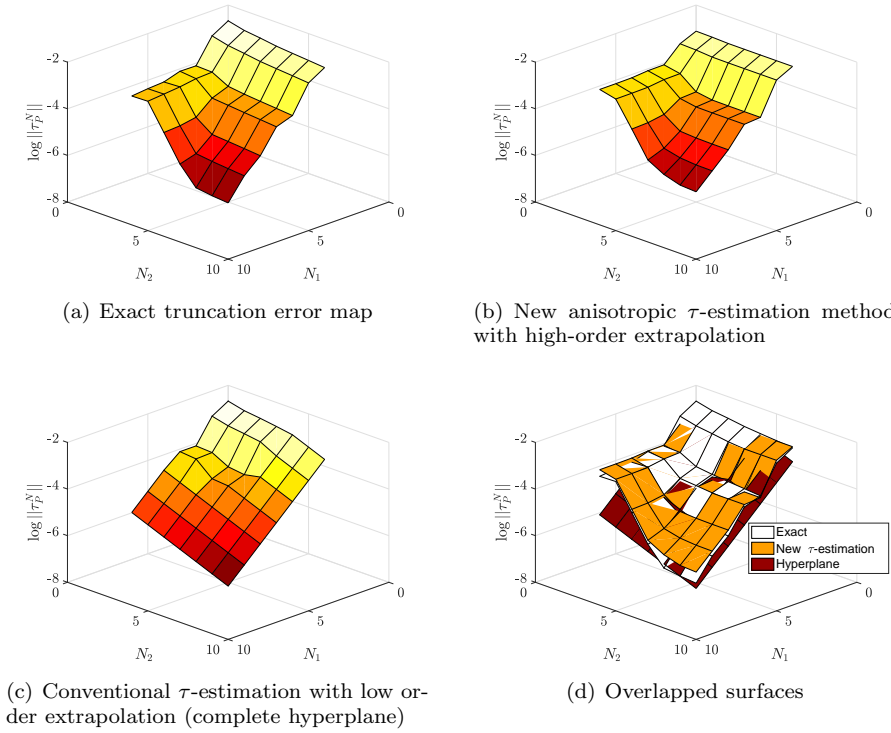


Fig. 7 Spatial representation of Two-dimensional anisotropic truncation error maps for the manufactured solutions test case

If we generate the truncation error map using the method of Kompenhans et al. [18] (section 2.4), we obtain Figure 8. Remark that although the method of Kompenhans et al. produces accurate results for $N_i < P$, it fails to predict the behavior of the truncation error for $N_i \geq P$. In fact, using this method the full truncation error map is not being generated, but only the extrapolations for the iso- N_i lines $N_1 = P_1 - 1$ and $N_2 = P_2 - 1$.

A close inspection of the values of the truncation error for a fixed polynomial order (dashed and dotted lines of Figure 8) can reveal details about the extrapolated map. Let us first analyze the truncation error for a fixed $N_2 = 4$. In Figure 9(a) we illustrate how $\tau_{5,5}^{N_1,4}$ is obtained using the new methodology of section 3.1: the anisotropic contributions of the truncation error, τ_1 and τ_2 , are used to generate independent trend lines and their values are then used to compute $\tau_{5,5}^{N_1,4}$. Figure 9(b) shows a comparison of this result with the exact truncation error and the one obtained using the method of Kompenhans et al.. It is remarkable that spectral convergence can be observed and both error estimators predict it.

Now, let us analyze the case of a fixed $N_1 = 4$. Figure 10(a) illustrates how $\tau_{5,5}^{4,N_2}$ is obtained. Notice how, in this case, for $N_2 \geq 3$ a stagnation in the decrease

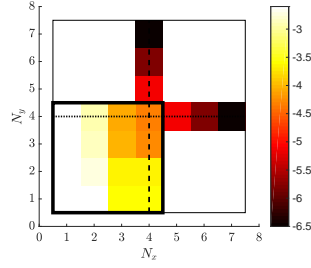
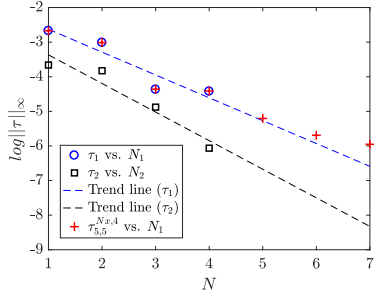
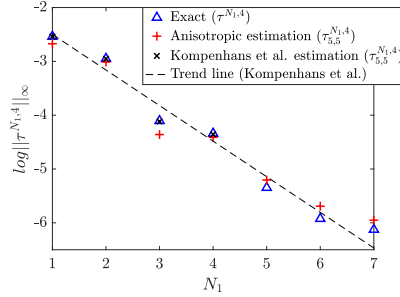


Fig. 8 Truncation error map estimated using the model of Kompenhans et al. [18] (logarithmic scale). Outside the black box are the extrapolated values of the estimated truncation error

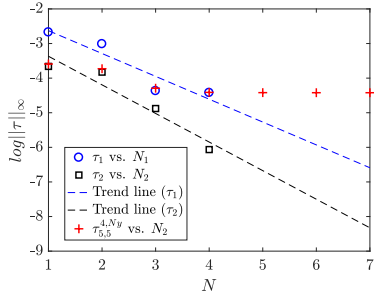


(a) Estimated τ_1 , τ_2 and $\tau_{5,5}^{Nx,4}$ with $P_1 = P_2 = 5$ (proposed anisotropic model)

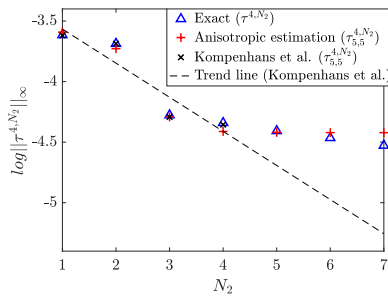


(b) Truncation error vs. N_1 for $N_2 = 4$

Fig. 9 Truncation error estimation using the new anisotropic model (a) and comparison with values obtained using the model of Kompenhans et al. [18] (b) for $N_2 = 4$ in element A (dotted line of Figure 8) - Logarithmic scale



(a) Estimated τ_1 , τ_2 and $\tau_{5,5}^{4,Ny}$ with $P_1 = P_2 = 5$ (proposed anisotropic model)



(b) Truncation error vs. N_2 for $N_1 = 4$

Fig. 10 Truncation error estimation using the new anisotropic model (a) and comparison with values obtained using the model of Kompenhans et al. [18] (b) for $N_1 = 4$ in element A (dashed line of Figure 8) - Logarithmic scale

ing rate of the truncation error occurs because

$$\|\tau_2(N_2 \geq 3)\|_\infty \leq \|\tau_1(N_1 = 4)\|_\infty. \quad (64)$$

Figure 10(b) shows a comparison of this result with the exact truncation error and the one obtained using the method of Kompenhans et al.. Remark that the exact truncation error also exhibits the stagnation behavior for $N_2 \geq 3$, but a linear extrapolation of the values of τ would under-predict the truncation error for $N_2 > 4$. The reason is that spectral convergence can be expected for the decoupled terms (τ_i), but not necessarily for the total truncation error along lines of the map (Theorems 2 and 3). This simple example shows how the anisotropic error estimator formulated in this paper can generate more accurate representations of the truncation error map for $N_i \geq P_i$ than previous estimators.

4.3 *Non-isolated* truncation error vs. *isolated* truncation error

As was discussed above, both the *non-isolated* and the *isolated* truncation error can be approximated using the anisotropic method introduced in this paper. In this section, we analyze how both estimators perform with the new anisotropic approximation when driving a p-adaptation procedure. The fully converged solution of order $P_1 = P_2 = 5$ is used as the reference mesh for the anisotropic τ -estimation procedure with *high-order extrapolation* explained in section 3.3. Different truncation error thresholds are studied in the range $10^{-7} \leq \tau_{max} < 10^{-1}$, and the polynomial order is selected after the estimation so that the number of degrees of freedom is minimized (see Figure 6). The maximum polynomial order allowed in any direction is selected as $N_{max} = 10$, and the minimum polynomial order as $N_{min} = 1$.

Figure 11(a) shows the *non-isolated* truncation error that was achieved after the mesh adaptation as a function of the specified threshold (τ_{max}), and Figure 11(b) illustrates the *isolated* truncation error that was achieved for different values of τ_{max} . Two plateaux can be observed in both figures, one for $\tau_{max} \leq 10^{-5}$ and one for $\tau_{max} \geq 6 \times 10^{-3}$ as a consequence of the limiting polynomial orders. The first plateau corresponds to the minimum $\|\tau\|_\infty$ (and $\|\hat{\tau}\|_\infty$) that can be achieved when $N_1 = N_2 = N_{max} = 10$, and the second corresponds to the maximum $\|\tau\|_\infty$ (and $\|\hat{\tau}\|_\infty$) that can be achieved when $N_1 = N_2 = N_{min} = 1$ in every element. For the remaining specified thresholds both estimators perform reasonably well, being the *isolated* truncation error slightly better. The small gap between the ideal and achieved errors is attributed to small errors in the estimation procedure.

As these results show, controlling the *isolated* truncation error of a mesh also controls its *non-isolated* truncation error: a further advantage of the *isolated* estimator. In fact, we can write the *non-isolated* truncation error in terms of the *isolated* truncation error from the definitions in section 2.2, and appendixes A and B:

$$\tau^N = \hat{\tau}^N + \int_{\partial\Omega}^N \left(\mathcal{F}(\mathbf{I}^N \bar{\mathbf{q}}) \cdot \mathbf{n} - \mathcal{F}^*(\mathbf{I}^N \bar{\mathbf{q}}, \mathbf{I}^N \bar{\mathbf{q}}, \mathbf{n}) \right) \phi d\sigma. \quad (65)$$

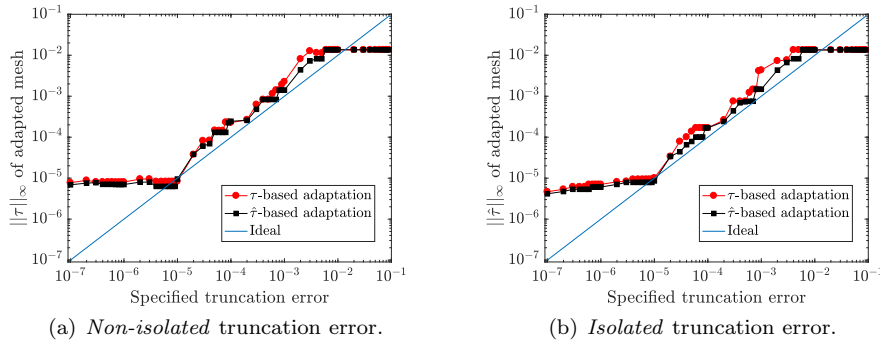


Fig. 11 Achieved *non-isolated* truncation error (a) and *isolated* truncation error (b) for adaptation procedures based on the *non-isolated* and the *isolated* truncation error for $N_{max} = 10$

Equation 65 suggests that the *isolated* truncation error is expected to control the *non-isolated* truncation error for sufficiently smooth solutions, for an appropriate choice of the numerical flux. This topic will be addressed in detail in future investigations.

Taking into account that the main difference of the *non-isolated* truncation error is that it is affected by neighboring elements, we can conclude that the *isolated* estimator is a better driver for p-adaptation methods than the *non-isolated* truncation error estimator. Namely, because it would be excessively expensive to evaluate every possible combination of polynomial orders for each element of the mesh *and* its neighbors in order to feed the p-adaptation procedure.

5 Conclusions

In this paper, we have studied truncation error estimators, their convergence properties and accuracy. The most important conclusions of this work are:

1. A new technique for evaluating the truncation error was developed which requires less computational resources in the estimation procedure than previous implementations. Furthermore, this technique allows computing extrapolations of the truncation error with enhanced accuracy compared with previous methods. This enables using coarser reference meshes, hence further improving the computational efficiency.
2. The presented method provides truncation error estimations that are accurate enough for performing p-adaptation, as shown in sections 4.1 and 4.3.
3. According to the analyses conducted in this paper, the *isolated* truncation error is better suited to drive a p-adaptation procedure than its *non-isolated* counterpart. In the first place, because the *non-isolated* error is affected by the discretization in other regions. Second, and as stated in remark 2, the *non-isolated* truncation error estimator imposes certain requirements for the extrapolation procedure to work well. This translates into a more expensive

τ -estimation. Furthermore, additional requirements are needed in order for the Theorem 1 to hold with the *non-isolated* truncation error.

4. The method of Kompenhans et al. [18], in which every combination of $N = (N_1, N_2, \dots, N_d)$ is directly evaluated for generating the truncation error map, performs slightly better at estimating the truncation error for $N_i < P_i$ than the proposed error estimator, but fails to predict the truncation error for $N_i \geq P_i$ accurately. A good compromise could be to generate the truncation error map for $N_i < P$ using the method of Kompenhans et al., but then changing to the fully decoupled method for generating the extrapolated map. In this case, however, additional evaluations of the discrete partial differential operator must be performed.

Acknowledgements The authors would like to thank David Kopriva for his friendly advise and cooperation. This project has received funding from the European Union’s Horizon 2020 Research and Innovation Program under the Marie Skłodowska-Curie grant agreement No 675008.

The authors acknowledge the computer resources and technical assistance provided by the *Centro de Supercomputación y Visualización de Madrid (CeSViMa)*.

References

1. Aftosmis, M.J.: Upwind method for simulation of viscous flow on adaptively refined meshes. *AIAA Journal* **32**(2), 268–277 (1994). DOI 10.2514/3.11981. URL <http://arc.aiaa.org/doi/10.2514/3.11981>
2. Berger, M.J.: Adaptive finite difference methods in fluid dynamics. In: *In Von Karman Inst. for Fluid Dynamics, Computational Fluid Dynamics 50 p (SEE N88-15951 08-34)* (1987)
3. Brandt, A., Livne, O.E.: *Multigrid Techniques: 1984 Guide with Applications to Fluid Dynamics, Revised Edition*. SIAM (2011). DOI 10.1137/1.9781611970753. URL <http://epubs.siam.org/doi/book/10.1137/1.9781611970753>
4. Canuto, C., Hussaini, M.Y., Quarteroni, A., Thomas Jr, A., Others: *Spectral methods in fluid dynamics*. Springer Science & Business Media (2012)
5. Choudhary, A., Roy, C.J.: Structured Mesh r-Refinement using Truncation Error Equidistribution for 1D and 2D Euler Problems. In: *21st AIAA Computational Fluid Dynamics Conference. American Institute of Aeronautics and Astronautics, Reston, Virginia, AIAA 2013-244*, pp. 1–15 (2013). DOI 10.2514/6.2013-2444
6. Cockburn, B., Karniadakis, G.E., Shu, C.W.: The Development of Discontinuous Galerkin Methods. *Discontinuous Galerkin Methods* **11**(0), 3–50 (2000). DOI 10.1007/978-3-642-59721-3_1. URL http://dx.doi.org/10.1007/978-3-642-59721-3_1
7. Deng, S.: Numerical simulation of optical coupling and light propagation in coupled optical resonators with size disorder. *Applied Numerical Mathematics* **57**(5-7 SPEC. ISS.), 475–485 (2007). DOI 10.1016/j.apnum.2006.07.001
8. Estep, D.: A Posteriori Error Bounds and Global Error Control for Approximation of Ordinary Differential Equations. *SIAM Journal on Numerical Analysis* **32**(1), 1–48 (1995)
9. Eva Casoni y Antonio Huerta: Shock capturing for discontinuous galerkin methods (2011). URL <http://www.tesisenred.net/handle/10803/51571>
10. F. Bassi, S. Rebay: A high-order accurate discontinuous finite element method for the numerical solution of the compressible Navier-Stokes equations. *Journal of Computational Physics* **131**, 267–279 (1997). DOI <http://dx.doi.org/10.1006/jcph.1996.5572>. URL <http://isn-csm.mit.edu/literature/1997-jcp-bassi.pdf>
11. Ferrer, E., Willden, R.H.: A high order Discontinuous Galerkin - Fourier incompressible 3D Navier-Stokes solver with rotating sliding meshes. *Journal of Computational Physics* **231**(21), 7037–7056 (2012). DOI 10.1016/j.jcp.2012.04.039. URL <http://dx.doi.org/10.1016/j.jcp.2012.04.039>

12. Fraysse, F., Redondo, C., Rubio, G., Valero, E.: Upwind methods for the Baer–Nunziato equations and higher-order reconstruction using artificial viscosity. *Journal of Computational Physics* **326**, 805–827 (2016). DOI 10.1016/j.jcp.2016.09.017. URL <http://dx.doi.org/10.1016/j.jcp.2016.09.017>
13. Fraysse, F., Valero, E., Ponsin, J.: Comparison of Mesh Adaptation Using the Adjoint Methodology and Truncation Error Estimates. *AIAA Journal* **50**(9), 1920–1932 (2012). DOI 10.2514/1.J051450. URL <http://arc.aiaa.org/doi/10.2514/1.J051450>
14. Georgoulis, E.: Discontinuous Galerkin methods on Shape-Regular and Anisotropic Meshes. *Philosophy* (2003). URL http://www.math.le.ac.uk/PEOPLE/eg64/papers/thesis{.}_main.pdf
15. Hartmann, R.: Error estimation and adjoint-based adaptation in aerodynamics. *European Conference on Computational Fluid Dynamics* pp. 1–14 (2006)
16. Hartmann, R., Houston, P.: Adaptive Discontinuous Galerkin Finite Element Methods for the Compressible Euler Equations. *Journal of Computational Physics* **183**(2), 508–532 (2002). DOI 10.1006/jcph.2002.7206. URL <http://linkinghub.elsevier.com/retrieve/pii/S0021999102972062>
17. Hesthaven, J.S., Warburton, T.: Nodal discontinuous Galerkin methods: algorithms, analysis, and applications. Springer Science & Business Media (2007)
18. Kompenhans, M., Rubio, G., Ferrer, E., Valero, E.: Adaptation strategies for high order discontinuous Galerkin methods based on Tau-estimation. *Journal of Computational Physics* **306**, 216–236 (2016). DOI 10.1016/j.jcp.2015.11.032. URL <http://dx.doi.org/10.1016/j.jcp.2015.11.032>
19. Kompenhans, M., Rubio, G., Ferrer, E., Valero, E.: Comparisons of p-adaptation strategies based on truncation- and discretisation-errors for high order discontinuous Galerkin methods. *Computers and Fluids* **139**, 36–46 (2016). DOI 10.1016/j.compfluid.2016.03.026. URL <http://dx.doi.org/10.1016/j.compfluid.2016.03.026>
20. Kopriva, D.: Implementing spectral methods for partial differential equations: Algorithms for scientists and engineers. Springer Science & Business Media (2009)
21. Kopriva, D.A.: Metric identities and the discontinuous spectral element method on curvilinear meshes. *Journal of Scientific Computing* **26**(3), 301–327 (2006). DOI 10.1007/s10915-005-9070-8
22. Kopriva, D.A., Woodruff, S.L., Hussaini, M.Y.: Computation of electromagnetic scattering with a non-conforming discontinuous spectral element method. *International Journal for Numerical Methods in Engineering* **53**(1), 105–122 (2002). DOI 10.1002/nme.394
23. Martin, R., Guillard, H.: A second order defect correction scheme for unsteady problems. *Computers and Fluids* **25**(1), 9–27 (1996). DOI 10.1016/0045-7930(95)00027-5
24. Mavriplis, C.: Nonconforming Discretizations and a Posteriori Error Estimators for Adaptive Spectral Element Techniques (1989). URL <http://hdl.handle.net/1721.1/14526>
25. Mavriplis, C.: Adaptive mesh strategies for the spectral element method. *Institute for Computer Applications in Science and Engineering* pp. 1–19 (1992). URL <http://www.sciencedirect.com/science/article/pii/S0045782594800103>
26. Minoli, C.A.A., Kopriva, D.A.: Discontinuous Galerkin spectral element approximations on moving meshes. *Journal of Computational Physics* **230**(5), 1876–1902 (2011). DOI 10.1016/j.jcp.2010.11.038. URL <http://dx.doi.org/10.1016/j.jcp.2010.11.038>
27. Oberkampf, W.L., Roy, C.J.: Verification and validation in scientific computing. Cambridge University Press (2010)
28. Persson, P.O., Peraire, J.: Sub-Cell Shock Capturing for Discontinuous Galerkin Methods. 44th AIAA Aerospace Sciences Meeting and Exhibit pp. 1–13 (2006). DOI 10.2514/6.2006-112. URL <http://arc.aiaa.org/doi/10.2514/6.2006-112>
29. Phillips, T., Delaga, J., Roy, C., Borggaard, J.: Finite volume solution reconstruction methods for truncation error estimation. 21st AIAA Computational Fluid Dynamics Conference (2013). DOI 10.2514/6.2013-3090
30. Phillips, T.S.: Residual-based Discretization Error Estimation for Computational Fluid Dynamics Residual-based Discretization Error Estimation for Computational Fluid Dynamics. Ph.D. thesis, Virginia Polytechnic Institute and State University (2014). URL <https://vtechworks.lib.vt.edu/handle/10919/50647>
31. Phillips, T.S., Roy, C.J.: Residual Methods for Discretization Error Estimation. 20th AIAA Computational Fluid Dynamics Conference **3870**(27-30), 665 (2011)
32. Phillips, T.S., Roy, C.J.: A New Extrapolation-Based Uncertainty Estimator for Computational Fluid Dynamics. *Journal of Verification, Validation and Uncertainty Quantification* **1**(4), 041,006 (2017). DOI 10.1115/1.4035666. URL <http://verification.asmedigitalcollection.asme.org/article.aspx?doi=10.1115/1.4035666>

33. Pierce, N.A., Giles, M.B.: Adjoint and defect error bounding and correction for functional estimates. *Journal of Computational Physics* **200**(2), 769–794 (2004). DOI 10.1016/j.jcp.2004.05.001
34. Rasetarinera, P., Hussaini, M.: An Efficient Implicit Discontinuous Spectral Galerkin Method. *Journal of Computational Physics* **172**(2), 718–738 (2001). DOI 10.1006/jcph.2001.6853. URL <http://linkinghub.elsevier.com/retrieve/pii/S0021999101968536>
35. Remacle, J.F., Flaherty, J.E., Shephard, M.S.: An Adaptive Discontinuous Galerkin Technique with an Orthogonal Basis Applied to Compressible Flow Problems. *Society for Industrial and Applied Mathematics. SIAM Review* **45**(1), 53–72 (2003)
36. Rivière, B.: Discontinuous Galerkin Methods for Solving Elliptic and Parabolic Equations Theory and Implementation. SIAM (2008). DOI 10.1137/1.9780898717440. URL <http://epubs.siam.org/doi/pdf/10.1137/1.9780898717440.appb%7D5Cnhttp://epubs.siam.org/doi/book/10.1137/1.9780898717440>
37. Roache, P.J.: Verification and validation in computational science and engineering, vol. 895. Hermosa Albuquerque, NM (1998)
38. Roe, P.L.: Approximate Riemann solvers, parameter vectors, and difference schemes. *Journal of Computational Physics* **43**(2), 357–372 (1981). DOI 10.1016/0021-9991(81)90128-5
39. Roy, C.: Review of Discretization Error Estimators in Scientific Computing. In: 48th AIAA Aerospace Sciences Meeting Including the New Horizons Forum and Aerospace Exposition. American Institute of Aeronautics and Astronautics, Reston, Virginia (2010). DOI 10.2514/6.2010-126. URL <http://arc.aiaa.org/doi/10.2514/6.2010-126>
40. Rubio, G., Fraysse, F., De Vicente, J., Valero, E.: The estimation of truncation error by τ -estimation for Chebyshev spectral collocation method. *Journal of Scientific Computing* **57**(1), 146–173 (2013). DOI 10.1007/s10915-013-9698-8
41. Rubio, G., Fraysse, F., Kopriva, D.A., Valero, E.: Quasi-a priori truncation error estimation in the DGSEM. *Journal of Scientific Computing* **64**(2), 425–455 (2015). DOI 10.1007/s10915-014-9938-6
42. Rubio Calzado, G.: Truncation error estimation in the Discontinuous Galerkin Spectral Element Method. Ph.D. thesis, Universidad Politécnica de Madrid. School of Aeronautics (ETSIAE) (2015)
43. Syrakos, A., Efthimiou, G., Bartzis, J.G., Goulas, A.: Numerical experiments on the efficiency of local grid refinement based on truncation error estimates. *Journal of Computational Physics* **231**(20), 6725–6753 (2012). DOI 10.1016/j.jcp.2012.06.023
44. Syrakos, A., Goulas, A.: Finite volume adaptive solutions using SIMPLE as smoother. *International Journal for Numerical Methods in Fluids* **52**(11), 1215–1245 (2006). DOI 10.1002/flid.1228
45. Toro, E.F.: Riemann solvers and numerical methods for fluid dynamics: a practical introduction. Springer Science & Business Media (2013)
46. Venditti, D.A., Darmofal, D.L.: Grid Adaptation for Functional Outputs: Application to Two-Dimensional Inviscid Flows. *Journal of Computational Physics* **176**(1), 40–69 (2002). DOI 10.1006/jcph.2001.6967. URL <http://linkinghub.elsevier.com/retrieve/pii/S0021999101969670>
47. Wang, Z., Fidkowski, K., Abgrall, R., Bassi, F., Caraeni, D., Cary, A., Deconinck, H., Hartmann, R., Hillewaert, K., Huynh, H., Kroll, N., May, G., Persson, P.O., van Leer, B., Visbal, M.: High-order CFD methods: current status and perspective. *International Journal for Numerical Methods in Fluids* **72**(8), 811–845 (2013). DOI 10.1002/flid.3767
48. Zienkiewicz, O.C.: The background of error estimation and adaptivity in finite element computations. *Computer Methods in Applied Mechanics and Engineering* **195**(4-6), 207–213 (2006). DOI 10.1016/j.cma.2004.07.053

A Isolated truncation error dependence on interpolation error

According to definition 5 and equation 34, the *isolated* truncation error in the DGSEM can be expressed for any basis function ϕ in an element e as

$$\hat{\tau}^N|_{\Omega^e} = \hat{\mathcal{R}}(\mathbf{I}^N \mathbf{q}) = \int_{\Omega^e}^N \mathbf{s}^N \phi d\Omega + \int_{\Omega^e}^N \mathcal{F}^N \cdot \nabla \phi d\Omega - \int_{\partial\Omega^e}^N \mathcal{F}^N \cdot \mathbf{n} \phi d\sigma, \quad (66)$$

where the superindex N on the integrals indicates that they are approximated with a Gaussian quadrature of order N and the superindex e has been dropped for readability. Since the DGSEM

is a collocation method, the value computed with equation 66 corresponds to the *isolated* truncation error on the node of the basis function ϕ . The terms \mathbf{s}^N and \mathcal{F}^N can be expressed in terms of the interpolation error as

$$\mathcal{F}^N = \mathbf{I}^N \mathcal{F}(\bar{\mathbf{q}}) = \mathcal{F}(\bar{\mathbf{q}}) - \varepsilon_{\mathcal{F}}^N, \quad \mathbf{s}^N = \mathbf{I}^N \mathbf{s} = \mathbf{s} - \varepsilon_{\mathbf{s}}^N. \quad (67)$$

Inserting equation 67 into 66, integrating by parts, and expressing everything with $L_2(\Omega)$ inner product notation we obtain,

$$\hat{\tau}^N|_{\Omega^e} = - \left(\varepsilon_{\mathbf{s}}^N, \phi \right)_{\Omega^e}^N + \left(\nabla \cdot \varepsilon_{\mathcal{F}}^N, \phi \right)_{\Omega^e}^N + \mathcal{O} \left(e_f^N \right), \quad (68)$$

where $(\cdot, \cdot)_{\Omega^e}^N$ stands for the L_2 product operator evaluated with a quadrature of order N in the domain Ω^e . The first term on the right-hand side vanishes since the value of $\varepsilon_{\mathbf{s}}^N$ is zero on the quadrature nodes (the DGSEM is a collocation method). Furthermore, it is reasonable to neglect the quadrature error since it is of a lower order of magnitude than the value of the integral. Therefore, we obtain

$$\hat{\tau}^N|_{\Omega^e} \approx \left(\nabla \cdot \varepsilon_{\mathcal{F}}^N, \phi \right)_{\Omega^e}^N. \quad (69)$$

B Anisotropic *non-isolated* truncation error estimation

In this section, we show briefly that the *non-isolated* truncation error can be estimated anisotropically using theorem 1. In order to do so, we need some additional assumptions.

B.1 Additional assumptions

As in section 3.1, following assumptions are a consequence of the tensor product basis functions of the DGSEM and hold for sufficiently smooth solutions in the asymptotic range:

- (c) The discretization error has an anisotropic behavior and, therefore, can be decoupled in directional components. For the 2D case:

$$\varepsilon^{N_1 N_2} = \varepsilon_1^{N_1 N_2} + \varepsilon_2^{N_1 N_2}. \quad (70)$$

As in (a), ε_i is the projection of the global discretization error, ε , into a local direction, i .

- (d) The *locally-generated* discretization error in each direction depends only on the polynomial order in that direction:

$$\varepsilon_{\Omega, i}^{N_1 N_2} = \varepsilon_{\Omega, i}^{N_1 N_2}(N_i) \quad (71)$$

Similar as in remark 2, and for reasons that will become clear at the end of the proof, following additional assumption is required:

- (e) The τ -estimation procedure is performed element-wise while keeping the polynomial order in other elements *sufficiently* high so that:

$$\left\| \varepsilon_{\partial\Omega}^N \right\| \ll \left\| \varepsilon_{\Omega}^N \right\| \quad (72)$$

As (a) and (b), assumptions (c) and (d) also follow from the work of Rubio et al. [41, 42]. Remark that assumptions (a), (b), (c) and (d) are consistent with the dependence of the *non-isolated* truncation error on the discretization error (equation 30).

Let us note that the assumption (d) implies that, for smooth solutions in the asymptotic range, the discretization error in one direction does not change considerably when the polynomial order in another direction is changed:

$$\begin{aligned} \varepsilon_j^{N_i P_j} &\approx \varepsilon_j^{P_i P_j}, \\ \varepsilon_i^{N_i P_j} &\neq \varepsilon_i^{P_i P_j}, \end{aligned} \quad (73)$$

with $i \neq j$, and $1 \leq i, j \leq 2$.

Proof.

Following the same procedure as in Appendix A, according to definition 4 and equation 28, the *non-isolated* truncation error in the DGSEM can be expressed for any basis function ϕ in an element e as

$$\tau^N|_{\Omega^e} = \mathcal{R}(\mathbf{I}^N \bar{\mathbf{q}}) = \int_{\Omega^e} \mathbf{s}^N \phi d\Omega + \int_{\Omega^e} \mathcal{F}(\mathbf{I}^N \bar{\mathbf{q}}) \cdot \nabla \phi d\Omega - \int_{\partial\Omega^e} \mathcal{F}^*(\mathbf{I}^N \bar{\mathbf{q}}, \mathbf{I}^N \bar{\mathbf{q}}^-, \mathbf{n}) \phi d\sigma, \quad (74)$$

where $\bar{\mathbf{q}}^-$ is the external (neighbor element's) solution and the superindex "e" has been dropped for the local solution. Since the DGSEM is a collocation method, the value computed with equation 74 corresponds to the *non-isolated* truncation error on the node of the basis function ϕ . After inserting the definition of discretization error (def. 2), $\bar{\mathbf{q}} = \bar{\mathbf{q}}^N + \epsilon^N$, and expanding the fluxes using Taylor series we obtain

$$\tau^N|_{\Omega^e} \approx \int_{\Omega^e} \frac{\partial \mathcal{F}}{\partial \mathbf{q}} \Big|_{\bar{\mathbf{q}}^N} \epsilon^N \cdot \nabla \phi d\Omega - \int_{\partial\Omega^e} \frac{\partial \mathcal{F}^*}{\partial \mathbf{q}} \Big|_{\bar{\mathbf{q}}^N, \bar{\mathbf{q}}^N, \mathbf{n}} \epsilon^N \phi d\sigma - \int_{\partial\Omega^e} \frac{\partial \mathcal{F}^*}{\partial \mathbf{q}^-} \Big|_{\bar{\mathbf{q}}^N, \bar{\mathbf{q}}^N, \mathbf{n}} \epsilon^N \phi d\sigma, \quad (75)$$

where the interpolant of the discretization error is omitted for readability ($\mathbf{I}^N \epsilon^N \rightarrow \epsilon^N$), ϵ^N is the discretization error of the element e , and ϵ^N is the discretization error of a neighbor element connected through the surface $\partial\Omega$. Notice that, for the sake of readability, the symbol for the external polynomial orders is the same as of the internal ones, i.e. N , although they can be different.

We now want to approximate the *non-isolated* truncation error through τ -estimation. We part from the definition of the discretization error (equation 20). Adding and subtracting the discrete solution on a higher order grid, \mathbf{q}^P , yields

$$\begin{aligned} \epsilon^N &= \bar{\mathbf{q}} - \bar{\mathbf{q}}^P + \bar{\mathbf{q}}^P - \bar{\mathbf{q}}^N \\ \epsilon^N &= \epsilon^P + \bar{\mathbf{q}}^P - \bar{\mathbf{q}}^N. \end{aligned}$$

Reorganizing we have

$$\bar{\mathbf{q}}^P = \bar{\mathbf{q}}^N + \epsilon^N - \epsilon^P. \quad (76)$$

Therefore, the τ -estimation yields

$$\begin{aligned} \tau_P^N|_{\Omega^e} = \mathcal{R}(\mathbf{I}^N \bar{\mathbf{q}}^P) &\approx \int_{\Omega^e} \frac{\partial \mathcal{F}}{\partial \mathbf{q}} \Big|_{\bar{\mathbf{q}}^N} (\epsilon^N - \epsilon^P) \cdot \nabla \phi d\Omega - \int_{\partial\Omega^e} \frac{\partial \mathcal{F}^*}{\partial \mathbf{q}} \Big|_{\bar{\mathbf{q}}^N, \bar{\mathbf{q}}^N, \mathbf{n}} (\epsilon^N - \epsilon^P) \phi d\sigma \\ &\quad - \int_{\partial\Omega^e} \frac{\partial \mathcal{F}^*}{\partial \mathbf{q}^-} \Big|_{\bar{\mathbf{q}}^N, \bar{\mathbf{q}}^N, \mathbf{n}} (\epsilon^N - \epsilon^P) \phi d\sigma. \quad (77) \end{aligned}$$

Since it is possible to decouple the discretization error inside our analyzed element in a *locally-generated* and an *externally-generated* component (equation 21), equation 77 can be rewritten as

$$\begin{aligned} \tau_P^N|_{\Omega^e} &\approx \int_{\Omega^e} \frac{\partial \mathcal{F}}{\partial \mathbf{q}} \Big|_{\bar{\mathbf{q}}^N} (\epsilon_{\Omega}^N - \epsilon_{\Omega}^P) \cdot \nabla \phi d\Omega - \int_{\partial\Omega^e} \frac{\partial \mathcal{F}^*}{\partial \mathbf{q}} \Big|_{\bar{\mathbf{q}}^N, \bar{\mathbf{q}}^N, \mathbf{n}} (\epsilon_{\Omega}^N - \epsilon_{\Omega}^P) \phi d\sigma \\ &\quad + \int_{\Omega^e} \frac{\partial \mathcal{F}}{\partial \mathbf{q}} \Big|_{\bar{\mathbf{q}}^N} (\epsilon_{\partial\Omega}^N - \epsilon_{\partial\Omega}^P) \cdot \nabla \phi d\Omega - \int_{\partial\Omega^e} \frac{\partial \mathcal{F}^*}{\partial \mathbf{q}} \Big|_{\bar{\mathbf{q}}^N, \bar{\mathbf{q}}^N, \mathbf{n}} (\epsilon_{\partial\Omega}^N - \epsilon_{\partial\Omega}^P) \phi d\sigma \\ &\quad - \int_{\partial\Omega^e} \frac{\partial \mathcal{F}^*}{\partial \mathbf{q}^-} \Big|_{\bar{\mathbf{q}}^N, \bar{\mathbf{q}}^N, \mathbf{n}} (\epsilon^N - \epsilon^P) \phi d\sigma. \quad (78) \end{aligned}$$

Equation 78 holds even for anisotropic representations, i.e. $N = (N_1, N_2, N_3)$ and $P = (P_1, P_2, P_3)$. Remark that if the polynomial order of the elements that are not being analyzed

is maintained as high as in the reference mesh, $\epsilon_{\partial\Omega}^P$ cancels out $\epsilon_{\partial\Omega}^N$ and $\epsilon^N - \epsilon^P \approx 0$. I.e., the τ -estimation provides the *locally-generated* truncation error.

Let us now consider the case of 2D anisotropic coarsening in the direction i ($\mathbf{N} = (N_i, P_j)$, $\mathbf{P} = (P_i, P_j)$). Taking into account assumptions (c) and (d), we obtain

$$\begin{aligned} \tau_{\mathbf{P}}^{\mathbf{N}}|_{\Omega^e} &\approx \int_{\Omega^e}^{\mathbf{N}} \frac{\partial \mathcal{F}}{\partial \mathbf{q}} \Big|_{\bar{\mathbf{q}}^{\mathbf{N}}} (\epsilon_{\Omega,i}^{\mathbf{N}} - \epsilon_{\Omega,i}^{\mathbf{P}}) \cdot \nabla \phi d\Omega - \int_{\partial\Omega^e}^{\mathbf{N}} \frac{\partial \mathcal{F}^*}{\partial \mathbf{q}} \Big|_{\bar{\mathbf{q}}^{\mathbf{N}}, \bar{\mathbf{q}}^{\mathbf{N}}, \mathbf{n}} (\epsilon_{\Omega,i}^{\mathbf{N}} - \epsilon_{\Omega,i}^{\mathbf{P}}) \phi d\sigma \\ &+ \int_{\Omega^e}^{\mathbf{N}} \frac{\partial \mathcal{F}}{\partial \mathbf{q}} \Big|_{\bar{\mathbf{q}}^{\mathbf{N}}} (\epsilon_{\partial\Omega}^{\mathbf{N}} - \epsilon_{\partial\Omega}^{\mathbf{P}}) \cdot \nabla \phi d\Omega - \int_{\partial\Omega^e}^{\mathbf{N}} \frac{\partial \mathcal{F}^*}{\partial \mathbf{q}} \Big|_{\bar{\mathbf{q}}^{\mathbf{N}}, \bar{\mathbf{q}}^{\mathbf{N}}, \mathbf{n}} (\epsilon_{\partial\Omega}^{\mathbf{N}} - \epsilon_{\partial\Omega}^{\mathbf{P}}) \phi d\sigma \\ &- \int_{\partial\Omega^e}^{\mathbf{N}} \frac{\partial \mathcal{F}^*}{\partial \mathbf{q}} \Big|_{\bar{\mathbf{q}}^{\mathbf{N}}, \bar{\mathbf{q}}^{\mathbf{N}}, \mathbf{n}} (\epsilon^{\mathbf{N}} - \epsilon^{\mathbf{P}}) \phi d\sigma. \end{aligned} \quad (79)$$

Finally, if assumption (c) and (e) hold, the anisotropic version of equation 78 ($N = (N_1, N_2, N_3)$) can be reconstructed by summing all the directional components (equation 79) if the quadrature errors are neglected. I.e., we recover equation 42:

$$\tau^{N_1 N_2} \approx \tau_{P_1 P_2}^{N_1 P_2} + \tau_{P_1 P_2}^{P_1 N_2} \quad (80)$$

□

C The Navier-Stokes equations

The compressible Navier-Stokes equations in conservative form can be written in non-dimensional form as

$$\mathbf{q}_t + \nabla \cdot (\mathcal{F}^a - \mathcal{F}^\nu) = \mathbf{s}, \quad (81)$$

where the conserved variables are $\mathbf{q} = (\rho, \rho u, \rho v, \rho w, \rho e)^T$ (ρ is the density; u , v and w are the velocity components; and e is the specific total energy), \mathbf{s} is an external source term, and \mathcal{F}^a and \mathcal{F}^ν are called the advective and diffusive flux dyadic tensors, respectively, which depend on \mathbf{q} . Expanding the fluxes in Cartesian coordinates leads to the expression,

$$\mathbf{q}_t + \mathbf{f}_x^a + \mathbf{g}_y^a + \mathbf{h}_z^a - \frac{1}{\text{Re}} (\mathbf{f}_x^\nu + \mathbf{g}_y^\nu + \mathbf{h}_z^\nu) = \mathbf{s}. \quad (82)$$

Here, Re is the Reynolds number. The advective fluxes are then defined as

$$\mathbf{f}^a = \begin{bmatrix} \rho u \\ p + \rho u^2 \\ \rho uv \\ \rho uw \\ u(\rho e + p) \end{bmatrix}, \quad \mathbf{g}^a = \begin{bmatrix} \rho v \\ \rho uv \\ p + \rho v^2 \\ \rho vw \\ v(\rho e + p) \end{bmatrix}, \quad \mathbf{h}^a = \begin{bmatrix} \rho w \\ \rho uw \\ \rho vw \\ p + \rho w^2 \\ w(\rho e + p) \end{bmatrix}, \quad (83)$$

where the pressure p is computed using the calorically perfect gas approximation. On the other hand, the diffusive fluxes are defined as

$$\mathbf{f}^\nu = \begin{bmatrix} 0 \\ \tau_{xx} \\ \tau_{xy} \\ \tau_{xz} \\ u\tau_{xx} + v\tau_{xy} + w\tau_{xz} + \frac{\kappa}{(\gamma-1)\text{PrM}^2}T_x \end{bmatrix}, \quad (84)$$

$$\mathbf{g}^\nu = \begin{bmatrix} 0 \\ \tau_{yx} \\ \tau_{yy} \\ \tau_{yz} \\ u\tau_{yx} + v\tau_{yy} + w\tau_{yz} + \frac{\kappa}{(\gamma-1)\text{PrM}^2}T_y \end{bmatrix}, \quad (85)$$

$$\mathbf{h}^\nu = \begin{bmatrix} 0 \\ \tau_{zx} \\ \tau_{zy} \\ \tau_{zz} \\ u\tau_{zx} + v\tau_{zy} + w\tau_{zz} + \frac{\kappa}{(\gamma-1)\text{PrM}^2}T_z \end{bmatrix}, \quad (86)$$

where T is the temperature, γ is the heat capacity ratio, and κ is the thermal diffusivity. The nondimensional parameters are Pr, the Prandtl number; and M, the Mach number. The stress tensor components are computed using the Stokes hypothesis,

$$\tau_{ij} = \mu \left(\frac{\partial v_i}{\partial x_j} + \frac{\partial v_j}{\partial x_i} \right), \quad i \neq j \quad (87)$$

$$\tau_{ii} = 2\mu \left(\frac{\partial v_i}{\partial x_i} + \nabla \cdot \mathbf{V} \right), \quad (88)$$

with μ the fluid's viscosity, and \mathbf{V} the flow velocity. For the simulations in this paper we chose the typical parameters for air: Pr = 0.72, $\gamma = 1.4$, while μ and κ are calculated using Sutherland's law.